VNiVERSiDAD Ð SALAMANCA

CAMPUS DE EXCELENCIA INTERNACIONAL

Final Master's Project

Characterisation of the A005 capsule in the test cryostat by scanning with ^{241}Am, ^{60}Co, ^{137}Cs and ^{22}Na point sources.

Caracterización de la cápsula A005 en el criostato de test mediante el escaneado con fuentes puntuales de ^{241}Am, ^{60}Co, ^{137}Cs y ^{22}Na
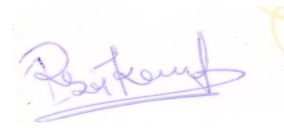

Gala González Briz

Project directed by:
Dr. Rajnikant Jashbhai Makwana

Interuniversity Nuclear Physics Master 2021-2022

Dr. Rajnikant Jashbhai Makwana, postdoctoral researcher at the Fundamental Physics Department of the University of Salamanca, authorises the presentation of the Final Master's Project entitled "Characterisation of the A005 capsule in the test cryostat by scanning with ^{241}Am, ^{60}Co, ^{137}Cs and ^{22}Na point sources.", carried out under his direction by Gala González Briz.

Salamanca, 21 October 2022.

Abstract

A new generation of position-sensitive γ spectrometry detectors are currently being promoted as they are important in nuclear and medical physics. Among them, AGATA (Advanced GAmma Tracking Array) stands out, an European research project that consists of the development of a 4π spectrometer based on the γ ray tracking technique. In other words, using electric segmentation technology in the crystals that compose the detector, it is possible to track the trajectory of the γ rays inside it, in order to reconstruct their emission position. The benefit of γ-ray tracking is that it is no longer necessary to incorporate Compton suppression shields, thus a larger solid angle can be covered and the efficiency of the system can be improved. In addition, AGATA aims to achieve unprecedented advances in spatial resolution. The spectrometer consists of 180 hexagonal HPGe (High Purity Germanium) crystals arranged in triple cluster structures. Additionally, each crystal is divided into 36 electrically isolated segments. Before incorporating the crystals into the spectrometer structure, it is necessary to characterise them i.e., to know their electrical response in each interaction position. To this end, the experimental characterisation of the A005 capsule is carried out through 2D and 3D scanning. The first one employs ^{241}Am, ^{60}Co and ^{137}Cs sources and intends to determine the real active volume of the crystal, defining the transverse boundaries that separate the segments and the position of the central hole, as well as its inclination within the cryostat. The 3D scanning is performed through SALSA (SAlamanca Lyso based Scanning Array), in which a ^{22}Na source is positioned between the AGATA capsule and a γ-camera composed of LYSO scintillator crystals. By operating with the detectors in coincidence, we take advantage of the collinearity of the annihilation photons, which also provides active collimation, to know the interaction position of the γ rays in the HPGe crystal. To evaluate the results, tracking reconstruction algorithms and PSA, i.e. pulse shape analysis, are employed. Indeed, each interaction position is characterised by the shape of the pulses in the segment where the detection occurs and in the neighbouring ones where induced signals are generated. Therefore, the aim of the 3D characterisation is to build a database that relates the interaction position of the γ rays in the AGATA crystal to their electrical response. A purpose-built scanning table is used, which contains an articulated arm that holds the γ-camera and the source holder, so that the whole setup can rotate around the capsule. In addition to the individual detector electronics for data acquisition, a complex logic circuit is set up for coincidence operation. Both processes run simultaneously, in parallel. On the other hand, we work on a simulation in

Geant4 that reproduces the experimental setup of the 3D scanning. Among the results it provides, it is derived that the efficiency of the system in coincidence is extremely low, 0.12%. Meanwhile, it is demonstrated that the individual detector efficiencies are lower than the geometrically estimated ones and also very low, since they do not reach 0.50%. Furthermore, the distribution of detections between the AGATA segments is analysed and it is found that it is not homogeneous, since the segments oriented towards the source record more photons than those on the opposite side. For this reason, it is concluded that in order to perform a correct characterisation of all the segments with the same statistics, it is required to rotate the crystal during the experimental measurements. As for the number of Compton scattering plus total absorption processes occurring in both detectors in each event, it is calculated that approximately 10 interactions occur per detection. All these magnitudes refer exclusively to the detection of annihilation photons, so that we establish energy gates in the range 505-517 keV in the analysis code. Experimentally, the proposed method for 2D scanning is validated. Although the equations defining the boundaries between segments are found, it is not possible to draw conclusions about the position and inclination of the central hole because the results are not sufficiently accurate due to the low statistics of the measurements. Regarding the 3D scanning, it is still in the measurement stage. Finally, resolution data on the different crystal segments are updated for energies 59.54 and 1332.5 keV.

Keywords

Resumen

En la actualidad, se están impulsando una nueva generación de detectores de espectrometría γ sensibles a la posición por su relevancia en física nuclear y física médica. Entre ellos, se encuentra AGATA (Advanced GAmma Tracking Array), un proyecto de investigación europeo que consiste en el desarrollo de un espectrómetro 4π basado en la técnica de tracking de rayos γ. Es decir, empleando tecnología de segmentación eléctrica en los cristales que componen el detector, es posible seguir la trayectoria de los rayos γ dentro de éste para reconstruir su posición de emisión. Gracias al seguimiento o tracking de los rayos γ, ya no es necesario incorporar escudos de supresión Compton, lo que permite cubrir un mayor ángulo sólido y posibilita una mejora en la eficiencia del sistema. Además, a través de AGATA se busca alcanzar avances en resolución espacial sin precedentes. El espectrómetro está constituido por 180 cristales hexagonales de HPGe (High Purity Germanium) organizados en estructuras de cluster triples. A su vez, cada cristal está dividido en 36 segmentos eléctricamente aislados. Antes de incorporar los cristales en la estructura del espectrómetro es necesario caracterizarlos, esto es, conocer su respuesta eléctrica en cada posición de interacción. Con ese fin se realiza la caracterización experimental de la cápsula A005, a través de un escaneado 2D y 3D. El primero de ellos utiliza fuentes de ^{241}Am, ^{60}Co y ^{137}Cs y pretende determinar el volumen activo real del cristal, definiendo los ejes transversales que separan los segmentos y la posición del orificio central, así como su inclinación dentro del criostato. El escaneado 3D se lleva a cabo a través de SALSA (SAlamanca Lyso based Scanning Array), en el que se posiciona una fuente de ^{22}Na entre la cápsula de AGATA y una γ-cámara compuesta por cristales centelleadores LYSO. Operando con los detectores en coincidencia, se aprovecha la colinealidad de los fotones de aniquilación, que proporciona además colimación activa, para conocer la posición de interacción de los rayos γ en el cristal de HPGe. Para estudiar los resultados se utilizan algoritmos de reconstrucción por tracking y PSA, esto es, análisis por la forma de los pulsos. En efecto, cada posición de interacción está caracterizada por la forma de los pulsos en el segmento donde se produce la detección y en los contiguos a éste, en los que se generan señales inducidas. Por tanto, el objetivo de la caracterización 3D es construir una base de datos que relacione la posición de interacción de los rayos γ en el cristal de AGATA con su respuesta eléctrica. Se utiliza una mesa de escaneado especialmente diseñada para ese fin, con un brazo articulado que sostiene la γ-cámara y el soporte de la fuente, de modo que el conjunto puede rotar entorno a la cápsula. Además de la electrónica individual de los detectores para la adquisición de datos, se establece un

complejo circuito lógico para la operación en coincidencia. Ambos procesos transcurren de manera simultánea, en paralelo. Por otro lado, se trabaja sobre una simulación en Geant4 que reproduce la estructura experimental del escaneado 3D. Entre los resultados que proporciona, se deriva que la eficiencia del sistema en coincidencia es muy baja, del 0.12%. Por su parte, se demuestra que las eficiencias individuales de los detectores son menores que las estimadas geométricamente y muy reducidas también, puesto que no alcanzan el 0.50%. Asimismo, se analiza la distribución de detecciones entre los segmentos de AGATA y se comprueba que no es homogénea puesto que los segmentos orientados hacia la fuente registran más fotones que los que se encuentran en la cara opuesta. Por ese motivo, se concluye que para realizar una correcta caracterización de todos los segmentos, con igual estadística, es necesario rotar el cristal durante las medidas experimentales. En cuanto al número de procesos de scattering Compton más absorción total que ocurren en ambos detectores en cada evento, se calcula que suceden aproximadamente 10 interacciones por detección. Todas estas magnitudes se refieren exclusivamente a la detección de fotones de aniquilación, por lo que se establecen ventanas energéticas en el intervalo 505-517 keV en el código de análisis. A nivel experimental, se valida el método propuesto para el escaneado 2D. Aunque se obtienen las ecuaciones que definen los ejes entre segmentos, no es posible sacar conclusiones sobre la posición e inclinación del orificio central porque los resultados no cuentan con la precisión suficiente debido a la baja estadística de las medidas. Por su parte, el escaneado 3D se encuentra en fase de medidas. Finalmente, se actualizan los datos sobre resolución en los diferentes segmentos del cristal para las energías 59.54 y 1332.5 keV.

Palabras clave

AGATA, detector segmentado, caracterización, espectrometría γ, escaneado 2D y 3D, simulación Geant4

Contents

List of Figures

List of Tables

1 Introduction

The incessant pursuit of knowledge about the atomic nucleus structure has made necessary the improvement and development of new technologies that can support such progress. Indeed, research in nuclear physics, as in other branches of science, advances as do the technological tools involved in the experiments. For this reason, in recent decades, the development of 4π radiation detectors, such as Euroball and Gammasphere, has contributed to obtaining a great deal of information about nuclear structure [1]. Nevertheless, such γ radiation spectrometers have significant limitations due to the solid angle they cover, as they are conditioned by the requirement for escape suppression shields. Because of that, a new generation of position-sensitive γ spectroscopy detectors based on the technique of tracking the γ rays in the crystal is being investigated, incorporating, in addition, new advances in crystal segmentation technology.

Currently, one of these detectors is AGATA, Advanced GAmma Tracking Array, a 4π spectrometer developed thanks to the collaboration between different research groups, such as IPHC in Strasbourg, Universities of Liverpool and York, GSI, IFIC, CSIC, IKP, CEA in Saclay, and many others. The AGATA total array is now installed at LNL-INFN (*Laboratori Nazionali di Legnaro - Istituto Nazionale di Fisica Nucleare*) because the current campaign is being carried out at the same laboratory (1). Actually, the AGATA project is working on the buildout of a set of highly segmented hyperpure germanium (HPGe) detectors that operate by the tracking of γ rays. It means, with these devices it would be possible to describe the trajectory of a γ-ray inside the crystal and reconstruct its emission position. This is possible because of the ability of highly segmented HPGe crystals to locate the interactions of photonic radiation in the detector with millimetre-accuracy.

Thanks to the tracking technique, Compton suppression shields, which limit the solid angle, are no longer necessary. The HPGe detectors are placed and thus cover a larger solid angle, which results in a very significant increase in efficiency, reaching unprecedented values in this field. In this way, the solid-angle coverage of full 4π is achieved almost completely. It also provides excellent angular resolution, which allows a very accurate Doppler correction [2]. For all these reasons, the AGATA detector is a very powerful and unique array that is proposed to be used not only in nuclear structure experiments but also in medical imaging research, due to its ability to reconstruct the position.
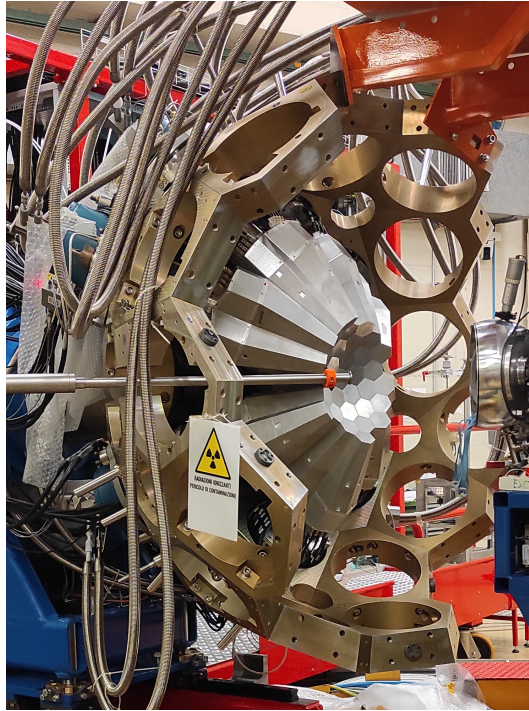
Figure 1: The AGATA spectrometer during the Legnaro campaign in June 2022.

However, to be able to use these new generation detectors in AGATA structure, it is necessary to carry out a prior characterisation of them. That is, we have first to investigate the real properties of the crystal, such as its active volume, efficiency, resolution, etc. The complete characterisation of the capsules, crystals, is carried out through experimental measurements with well-known sources, from which information of energy, position and time is obtained. Then comparison is made between experimental results and simulations that recreate the detector response, so pulse shape analysis (PSA) algorithms are required for further studies with AGATA.

1.1   AGATA array

The AGATA spectrometer consists of position-sensitive HPGe crystals, which allow tracking the path of the γ rays inside the detector and adding the partial energies deposited by the photons when they undergo multiple Compton scattering, even in interactions between different crystals. In terms of ge-

ometry, the total AGATA array has 180 hexagonal crystals arranged in a sphere [1]. In order to cover the largest possible solid angle (82% of 4π), crystals of three different geometries are used, although all capsules exhibit hexagonal cross-sections. According to their shape, they are classified into three groups: type A (in red), type B (in green) and type C (in blue). The AGATA device is composed of total 60 crystal sub-sets called triple-clusters, which consist of cryostats containing three crystals, one of each type. The clusters are used to support the three capsules, as a liquid nitrogen cooling medium and to support the first two pre-amplification stages. In addition, each crystal is formed by 36 electrically isolated segments, organised in six segments within six slices. The complete distribution of AGATA is as follows:
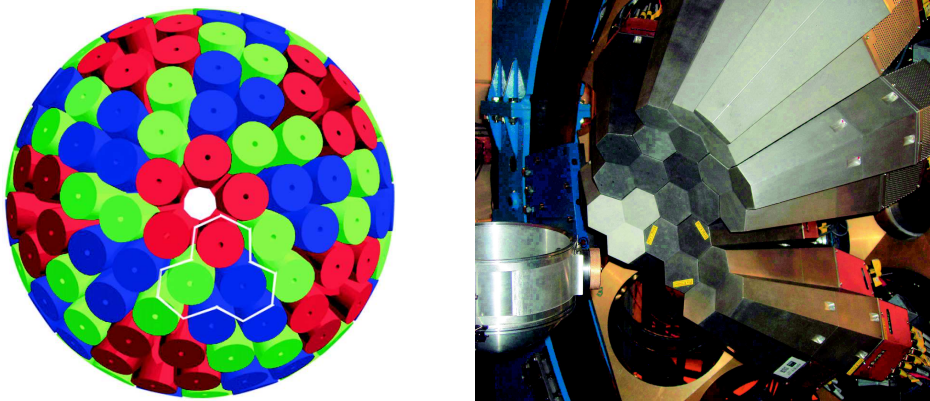
Figure 2: Left: AGATA configuration with the triple-cluster array composed of type A (red), B (green), C (blue) crystals. Right: The AGATA spectrometer for the GANIL phase during summer 2015, with 8 triple-clusters and 24 capsules.

The capsules consist of large n-type HPGe crystals with an impurity concentration between 0.4 and $1.8 \cdot 10^{10}$ cm^{-3}, tapered, coaxial and encapsulated, with segmentation technology. One of the main advantages of AGATA over other spectrometers is it maximises the efficiency for high-energy γ radiation, since the capsules have a coaxial design that contribute to a compact and thick HPGe coverage, so that a wide amount of detection material is available. Regarding the geometry, the capsules are conical in shape with a hexagonal cross-section at the front, which is a specially designed configuration to fit in an optimal way into the overall AGATA mosaic. In that way, this results in the best possible total solid angle coverage, which achieves a value of 82% of 4π sr. For its part, the distribution within each capsule is

---

[1]Currently, the AGATA spectrometer has 56 asymmetric capsules, including 18 type A, 19 type B and 19 type C.

such that the crystals are made up of 36 electrically isolated segments. These 36 segments are divided into 6 slices of 6 sectors each one. The summary information is given in the table below:

Number of triple clusters	60
Number of crystals per cluster	3
Number of segments per crystal	37 (36 + core)
Covered solid angle (%)	82
Number of channels	6660

Table 1: AGATA technical specifications [6]

It should be noted that the thickness of the foils has been optimised to achieve the best sensitivity and uniform distribution of the radiation interactions in the detector. In the central region of the capsule there is a tubular-shaped hole containing the n+ contact, associated with the core electronic channel. This contact collects the total signal, which corresponds to the interaction in the entire active volume. As the surfaces of the HPGe crystals are very sensitive, it is necessary to encapsulate and seal them inside an aluminium cover which protect them from damage in the material [3].

1.2   Properties of the A005 capsule

Like all other detectors that make up the AGATA spectrometer, the A005 capsule was manufactured by the Canberra company in France. The crystal consists of 36 electrically insulated segments arranged in 6 cross sections, rings. Each ring is identified by a number, from 1 to 6, and each of them is further subdivided into 6 sectors labelled with letters, from a to f, so that each segment is given by a letter and a number: a1, a2, ..., f6; see figure 3. In addition, the capsule has a central hole, core, where all the energy deposited on the crystal is collected, so that 37 signals are actually obtained in each measurement (36 from the segments plus the core). The high voltage required by the detector is applied through the core contact and it is isolated from the rest of the segments by ceramic materials.
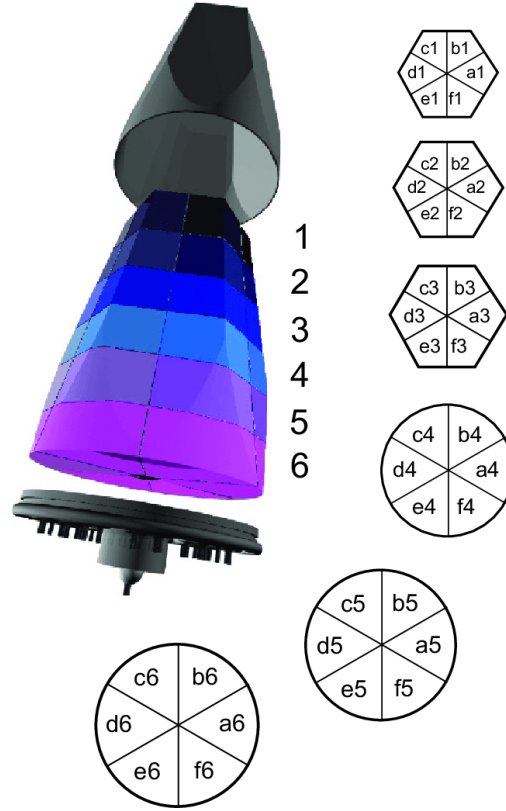
Figure 3: Diagram of segment labelling on an AGATA capsule. Along the axis, the crystal is divided into six rings, which are identified by numbers from 1 to 6. Each ring is further subdivided into six regions, labelled with letters from a to f.

As for the geometry of the capsule, it has a cylindrical shape at the rear, with a diameter of $80^{+0.7}_{-0.1}$ mm. Towards the front, the capsule tapers to a hexagonal conical shape. In other words, the crystal is cone-shaped, with a taper angle of 10°, and hexagonal section. The central hole has a diameter of 10 mm and a length of 77 mm, i.e. it is located from the back side to a distance of 13 mm from the front one. The glass has a length of 90 ± 1 mm and is segmented into six rings of 8, 13, 15, 18, 18, 18 and 18 mm of thickness, arranged from the front, the hexagonal side. These thicknesses have been selected for each slice in order to achieve an uniform distribution of the interactions of the γ radiation in the crystal and to optimise the sensitivity of the pulse shape. Regarding the transverse segmentation, the axes separating each segment pass through the centre of the crystal and through the middle of each hexagonal face, approximately, as it is shown in the picture 4. The weight of the bare germanium crystal is about 2 kg, [4].
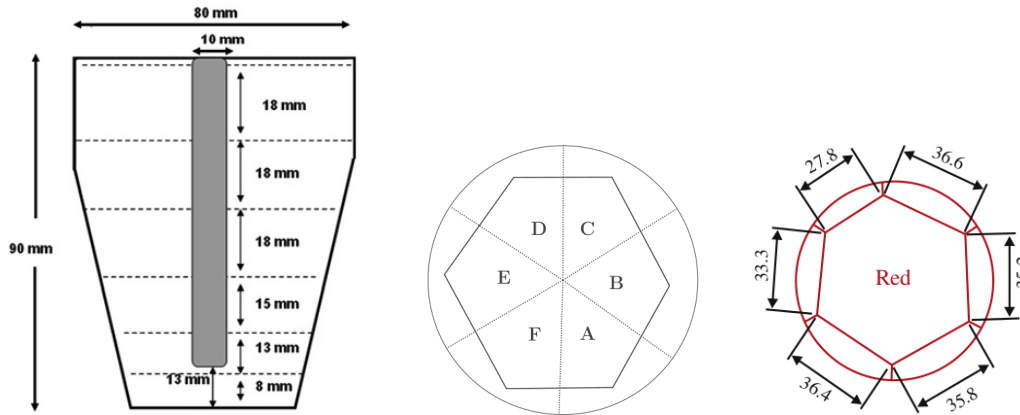
Figure 4: Left: Diagram of the lateral projection of the crystal, showing the central hole and the thicknesses of the segments, as well as other dimensions. Centre: Transversal section, revealing that the edges of each sector pass through the approximate midpoint of the crystal faces. Right: Transversal section of a type A (red) crystal, which states the length of each side of the lower hexagon. All dimensions are given in mm.

1.3   Semiconductor detectors

The detectors used for AGATA setup are HPGe, and it is known that HPGe are highly pure germanium semiconductors.

The structure of crystalline solids is such that electrons are shared between the different atoms that make up the crystal by forming covalent bonds. In fact, the structure of crystalline solids, such as silicon or germanium, is a perfectly organised lattice that repeats periodically and indefinitely until its boundaries to form a mono-crystal. Both germanium and silicon crystals have a face-centered-cubic lattice as its structure pattern. As far as electrons are concerned, their allowed energy levels are not discrete, as was in the case for single atoms, but are associated with large energy bands due to the atoms being contained in a lattice. The electrons are distributed in energy bands so that the last occupied one corresponds to the electrons in the outer shell of the atom, which is called the valence band. After it, the next-higher lying band is known as the conduction band. Between the valence band and the conduction band there is a region known as the gap where the forbidden energies are located. That is to say, in this energy interval, gap, no electron can be found because it is a region of forbidden energies. Nevertheless, if impurities are present in the material, the gap contains some allowed energy states. The size of the gap characterises the resistivity of a material, i.e. depending on the energy range of the gap, the substance will be a conductor,

an insulator or a semiconductor [3].

Three situations arise:

· In conductive materials the gap is zero and the valence band is not complete, so electrons can move freely.

· Insulating materials are characterised by a very high energy gap (typically over 5 eV) so that electrons cannot pass from the valence band to the conduction band. For energetic reasons, the electrons cannot leave the valence band, which is therefore full. As there are no free energy levels available, the electrons cannot move and there is no conduction in the material.

· Semiconductor materials are a middle ground between conductors and insulators. They have a small gap energy, so some electrons can cross from the valence band to the conduction band, which allows for a slight mobility of them. Numerically, band gaps in semiconductors are usually about 1 eV, such as silicon which has an energy gap of 1.17 eV or germanium of 0.74 eV, at 0 K.
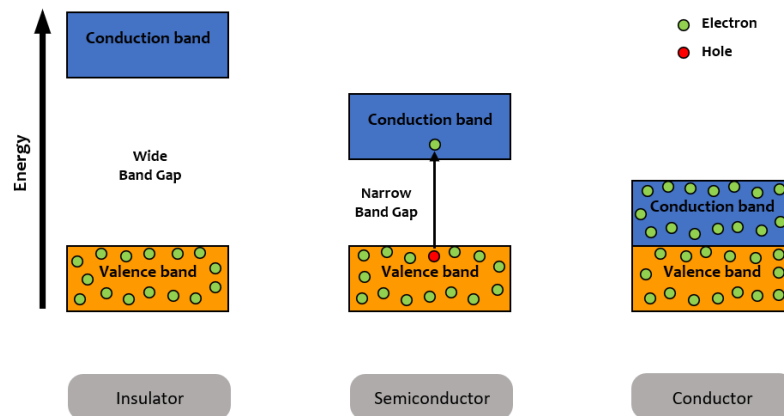
Figure 5: Band structure for electron energies according to the type of material: insulator, semiconductor and conductor.

In semiconductor materials, if the electrons in the valence band acquire a certain energy, such as thermal energy, they can bridge the gap and reach the conduction band. In this case, they leave vacancies in the conduction band known as holes. As these vacancies exist, electrons can move around to occupy them and, in turn, generate new holes. Thus, electrons can be

thought of as moving in the conduction band, while holes can also do in the valence band. That is why both electrons and holes contribute to the overall conductivity in the material. When using germanium detectors, it must be taken into account that they must be kept at very low temperature, cooled with liquid nitrogen. This is because germanium has a low gap, 0.66 eV at 300 K, and, at room temperature, the thermal energy is sufficient to generate electron-hole pairs, which give rise to current in the material. However, it is important that the current generated is only due to the interactions of the radiation with the sensitive material, without the influence of temperature. The aim of cooling with liquid nitrogen is to reduce this thermal contribution [3].

It has to be taken into account that the semiconductor materials are not perfectly pure, but contain impurities or defects in the crystal structure that condition the detection. In this sense, detectors often consist of semiconductor lattices doped with impurities, which are classified into two types:

- · Impurities that provide free holes in the crystalline structure of the semiconductor, which are those with three valence electrons, such as boron, aluminium, gallium or indium. They are known as acceptor impurities, because the holes can capture electrons. Materials in which acceptor impurities predominate are called p-type materials.

- · On the other hand, there are impurities that introduce free electrons into the semiconductor structure. These are those with five valence electrons, such as phosphorus, arsenic or antimony. They are called donor impurities, since they provide, they donate electrons. Materials in which donor impurities prevail are known as n-type materials [8].

Detection in semiconductor devices is based on the following mechanism:

Ionising radiation strikes the detector and interacts with the sensitive semiconductor material of which it is composed. At this point, the radiation gives up its energy to the electrons of the atoms that make up the crystalline structure of the semiconductor. If the energy is enough to overcome the gap, i.e. greater than or equal to the energy of the region of forbidden states, the electrons can be promoted from the valence band to the conduction one. In this case, electron-hole pairs are produced, as the electrons move into the conduction band and leave vacancies in the valence band. It is important to note that the number of electron-hole pairs produced is proportional to the energy deposited by the radiation in the detector. When a potential is applied between the limits of the detector, an electric field is generated and

causes the electrons and holes, i.e. an electric current, to move towards the electrodes. The electrodes are electronic devices where the charge of the electrons and holes is collected and translated into a measurable electrical pulse in an external circuit. That is, the ultimate aim of the detection process is the production of this pulse, since through its analysis in an outer circuit allows the characterisation of the initial incident radiation. In addition to the collection of electron-hole pairs at the electrodes, recombination can also occur within the detector, due to the presence of impurities or structural imperfections in the crystal. Impurities lead to particle recombination centres in the material, resulting in a lower charge collection at the electrodes than would be expected initially. The presence of impurities in the semiconductor causes energy levels to appear in the forbidden band gap. As a consequence, the impurities act as particle traps, since electrons can occupy these levels that are initially not allowed because they are inside the gap. They are interpreted as particle traps because they can capture electrons or holes and release them later.
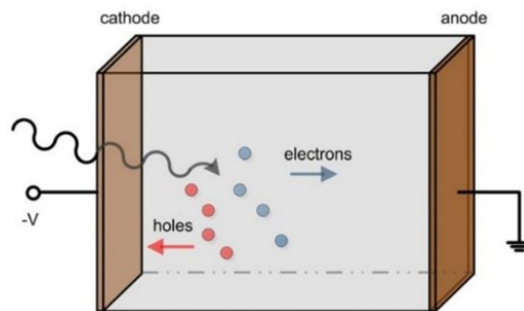
Figure 6: Diagram of the detection of ionising radiation in a semiconductor detector.

The subsequent analysis of the pulses provides information on the energy of the incident radiation, and on its intensity if a time study of the pulses is carried out. Moreover, it is important to supply the detector with a high voltage source to establish the electric field necessary for the displacement of the electrons and holes towards the electrodes.

1.3.1   High-purity germanium detectors

Advances in semiconductor crystal production equipment and techniques have made it possible to achieve germanium lattices with very high purity levels. In other words, germanium detectors are now manufactured with

high-purity crystals, or HPGe. While it is true that significant degrees of purity have been reached, today's crystals still contain impurities, both p- and n-type, as replacements for some lattice atoms. Numerically, the impurities present in high-purity germanium crystals are found in concentrations of the order of 10^{10} $atoms \cdot cm^{-3}$. In the electrodes, which are the electrical contacts where the charge is collected, boron is implanted in one side and lithium in the other.

In the AGATA spectrometer, all the crystals that make up the detectors are made of n-type HPGe. In addition, these impurities are in a specified concentration between 0.4 and $1.8 \cdot 10^{10}$ cm^{-3} [4]. As mentioned above, n-type materials are those in which donor impurities predominate, i.e., those that introduce free electrons into the semiconductor structure. As a consequence, in the band structure, a donor level is created near the conduction band. For primary research, n-type HPGe crystals are selected instead of p-type ones, since they have a lower sensitivity to neutron damage and a thinner entrance window which provides better spectroscopic performances for low energy γ-rays [3].

1.3.2   Segmentation. Highly segmented detectors

Segmentation is a very powerful tool in semiconductor detectors that consists of subdividing these devices into many readout channels. It requires highly integrated readout circuitry, as it can be compressed to fit small electrodes. Segmentation is a mechanism that offers numerous advantages over more conventional detection. On the one hand, it enhances the rate capability and the electronic noise. It also makes it possible to distinguish, to a greater extent, multiple tracks emitted at the same time into a small solid angle. On the other hand, segmentation allows a reduction in capacitance by reducing the area per electrode, which results in an improvement in sensitivity and energy resolution. Another advantage of segmentation lies in the enhancement of the radiation resistance [9].

As for the AGATA spectrometer, its crystals have an optimised configuration of the segments in such a way that a high sensitivity of the pulse shape is achieved while employing as few readout channels as possible [3].

1.4   LYSO crystals

The γ-camera used for the 3D scanning is composed by four detectors consisting of LYSO-type scintillator crystals coupled to position sensitive photomultiplier tubes (PSPMT). The crystals employed are lutetium yttrium oxyorthosilicate scintillators, hence the acronym LYSO, whose composition is $Lu_{2(1-x)}Y_{2x}SiO_5$. Together with lutetium oxyorthosilicate (LSO) crystals, they are the scintillators most widely used today in PET (Positron Emission Tomography) applications because of their convenient physical properties for the detection of the 511 keV annihilation photons, such as its high light output, high linear attenuation coefficient and short decay time [10].

LYSO crystals have intrinsic radioactive activity because they contain an unstable Lu isotope, ^{176}Lu [2]. The decay scheme of ^{176}Lu is given below:
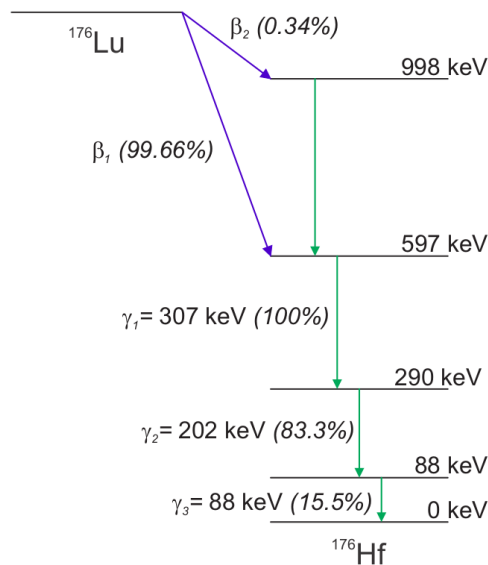
Figure 7: ^{176}Lu decay scheme.

[2]The intrinsic LYSO γ emissions affect the γ-camera measurements because one of the self-activity peaks appears at 508.66 keV, in the same energy window as the 511 keV peak of the annihilation photons. This 508.66 keV peak is due to the sum of the two in-cascade emissions of 201 and 306 keV from ^{176}Lu, and may spoil the reliability of the characterisation by interfering with the 511 keV peak. However, when measuring in time coincidence with another detector, the HPGe detector, the background due to the intrinsic LYSO emissions is significantly reduced, cleaning the spectrum so that only the contribution from the 511 keV annihilation photons appears [7] .

Naturally occurring lutetium contains 2.6% of ^{176}Lu which decays beta to excited states of ^{176}Hf, yielding a constant background signal.

The data for γ emissions due to decays of the ^{176}Lu isotope are presented in the following table:

Energy (keV)	Intensity (%)	Type	Origin	Start level	End level
306.82(8)	93.0(3)	γ	^{176}Hf	3	2
201.83(8)	78.0(4)	γ	^{176}Hf	2	1
88.36(2)	14.5(2)	γ	^{176}Hf	1	0
401.0(1)	0.4(1)	γ	^{176}Hf	4	3

Table 2: Data on ^{176}Lu isotope γ emissions.

2 Motivation

The AGATA project is based on the development of a position-sensitive spectrometer with unique characteristics: the aim is to achieve the highest spatial resolution using as few segments as possible. Indeed, one of the main challenges facing such a detector is to obtain significant advances in spatial resolution, using pulse shape analysis or comparison methods, without resorting to extremely fine segmentation.

In order to be able to work with the total spectrometer in nuclear physics experiments, it is necessary to have previously characterised the capsules that compose it. That is, before including the capsule in the complete structure of the detector, it is important to know its properties, such as its resolution or efficiency, and its response to photon detection. That is why the characterisation of the A005 capsule has to be done.

In addition to the University of Salamanca, there are several groups dedicated to the characterisation of the capsules, such as University of Liverpool, IPHC institute in Strasbourg or GSI. The scanning of the same capsules, such as the A005 one, by different research groups makes it possible to compare the different methods followed at each site, i.e. to compare the different scanning tables used to characterise the capsules. In this way, it is possible to determine which one provides the best results for each magnitude and to combine the data for a complete characterisation of the capsules. The Liverpool and Strasbourg tables are based on more mechanical procedures than the Salamanca one, which stands out for its use of active collimation and pulse shape analysis methods in 3D scanning. This study will allow to understand how the coincidence work and learn position scanning techniques.

In conclusion, AGATA is thouhgt to have unique qualities that will make it stand out from other detectors developed so far. The advances in resolution and solid angle that are expected to be achieved will make it possible, in the future, to carry out experiments in which significant progress will be made in our knowledge of the structure of nuclei. In other words, the AGATA spectrometer is a tool that will enable us to make advances in what is known at the nuclear level. Within this vision of the future, the characterisation of the capsules is a prior and fundamental step for the spectrometer to operate properly.

3 Development

The aim of this work is the characterisation, mostly geometrical, of the A005 capsule in the test cryostat. This is the first step in a much more complete characterisation of the detector and, at the same time, this is a small step in a larger project such as the AGATA spectrometer.

Through the AGATA project, the objective is to build a spectrometer that covers a large solid angle (82% of 4π) and it is a position-sensitive detector that can reconstruct the γ-ray emission point. One of the key features of such spectrometer is the spatial information it provides. That is why it is very important to know the real geometrical properties of the detector that makes up each capsule, such as its active volume, the position of the central hole, its inclination, etc. For this reason it is essential to carry out a correct geometrical characterisation of the HPGe crystal and this is the focus of this work.

In order to perform the characterisation of the A005 capsule, a series of measurements, in the form of scans, are made on a table set up for this purpose. The scans consist of measuring known radioactive sources, such as ^{241}Am, ^{60}Co, ^{137}Cs and ^{22}Na, placed in different positions of an array, and obtaining and analysing the spectrum recorded by each segment of the crystal. In other words, measurements are taken in a horizontal and a vertical distribution and the achieved results are interpreted to determine certain real geometrical properties of the HPGe crystal. In the following, a schematic of the scanning process of the A005 capsule is presented, which will be detailed in the section 3.5:

1. 2D horizontal scanning:

   · General: to provide a first reconstruction of the active volume of the lower crystal ring. We employ ^{241}Am.
   · Specific for identification of the transverse edges: we focus measurements on the limits of each segment in order to know their real boundaries. ^{241}Am is also used.
   · Specific on the central hole: the aim is to determine the real position of the central hole and its inclination with respect to the vertical axis, to correct it. ^{60}Co and ^{137}Cs sources are employed.

2. 3D scanning: performing a coincidence study, in which a γ-camera composed of LYSO crystals is used as a second detector.

The general procedure followed for each measurement in 2D scans is explained below:

The source of interest is placed on the source holder, which is located on the micrometric scanning table. The aim is to obtain a collimated beam of γ rays which is directed towards the detector. The micrometric screws are used to position the source at the desired point on a grid with x and y axes. On the computer, the acquisition is launched by selecting a series of configuration input parameters. After a certain time, typically between half an hour and an hour, the acquisition is stopped. The optimum measurement time for each scan has to be selected so as to obtain acceptable statistics without prolonging the measurements excessively, since a large number of measurements have to be made. From each acquisition, 37 spectra are obtained, one for each segment plus the core. The relevant information we are interested in for each one is the peak area of the emission of interest. In other words, the analysis of the data consists of locating in the spectrum the peak corresponding to the γ rays of the used source. Then, the Gaussian fit is performed and the area value is calculated. As it is known, the area is related to the number of counts detected by the crystal, and, for this reason, this magnitude is used to characterise the detector geometrically. As a collimated beam is employed, when the source is close to a segment, the count will be maximum in this segment, while in the rest it will be practically zero. Furthermore, when the source is positioned close to a segment edge or in the hole, the number of counts decreases very significantly. Thus, by obtaining the values of the peak area in each segment, the detector can be characterised. Depending on the target of each scanning, such as the edges of the segments or the hole, the spectra of some segments will be considered, as it will be seen below. In order to be able to compare between different measurements, the values of the area divided by the measurement time are actually used. That is, for each position, the relevant quantity to be studied is the area of the peak divided by the time of measurement. The raw data are represented in different ways to study the behaviour of the system and to define its shape.

3.1   Experimental setup

The experimental setup where the measurements are taken consists of a scanning table specially prepared and intended for the characterisation of the AGATA capsule. The scanning table has two heights and, on the lower one, there is a grid-shaped table where the source and the collimator are placed.

This table allows movement in both X and Y axes, and adjusts the position of the source by means of two micrometric screws, one for each axis. As mentioned above, the screws are micrometric, so they allow the position of the source, i.e. the collimated beam, to be set with high precision in microns. In addition, the grid table is located inside a larger structure containing an arm on which the γ-camera, made of LYSO crystals, is placed. This arm allows the movement of the γ-camera around the detector. In other words, the main elements of the structure are the grid table and the arm supporting the γ-camera, for the 3D scan. It is worth remembering that the structure is specially designed and built for the capsule scanning. On the micrometric grid, a structure supporting the γ source and the collimator is located. Collimators of 1 and 3 mm diameter are used to obtain a collimated beam of γ rays that interacts precisely at one position on the crystal.
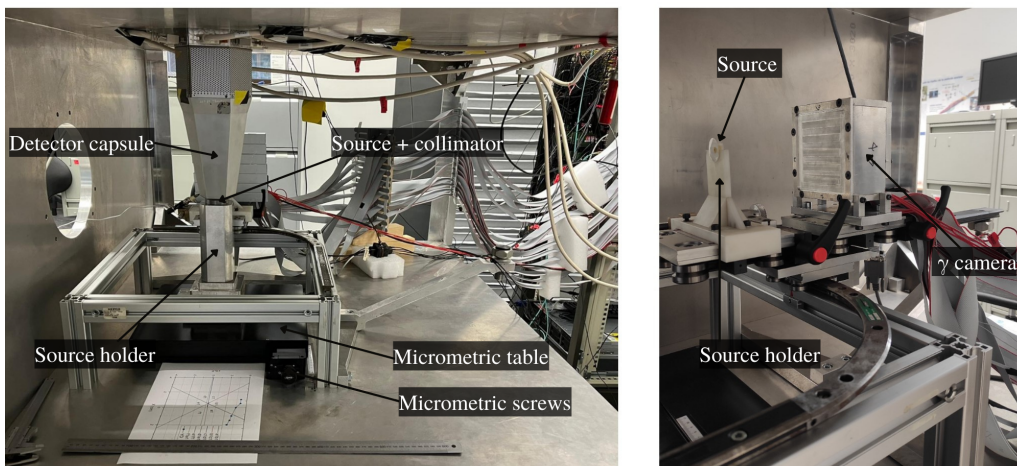
Figure 8: Photographs of the actual experimental set-up. Left: The image shows the scanning table, with the micrometric table, the source holder and the detector. Right: The picture shows the γ-camera together with the scanning arm supporting it and a source on another stand.

Above the grid structure, on the top of the table, it contains a circular hole specially centred on the origin of the XY axes where the detector is placed. In other words, to carry out the scanning, the detector is inserted through the top hole of the table, which is centred with respect to the grid axes. The diameter of the hole is such that it allows the detector capsule to pass through, but not the cryostat, which remains above it. Furthermore, the base of the hole has a structure of micrometric screws that allow, on the one hand, to fix and support the capsule to the table, and, on the other

hand, to set the inclination of the detector so that it is completely vertical with respect to the table.

The cryostat is connected to a liquid nitrogen tank, which recharges it every 8 hours. For proper operation, the HPGe crystals have to be kept at very low, cryogenic temperatures, so it is necessary to maintain them cold with liquid nitrogen. We dispose of an automatic refilling system that fills the cryostat of the capsule with liquid nitrogen from the tank connected to it. The system consists of an electronic valve and controller that initiates refills every 8 hours and in case of emergency. To monitor the temperature of the detector and the room, temperature sensors such as PT100 and thermocouples are connected to the electronics. This ensures the correct cooling of the crystals, because if the temperature rises above a certain threshold, an emergency refill is triggered.
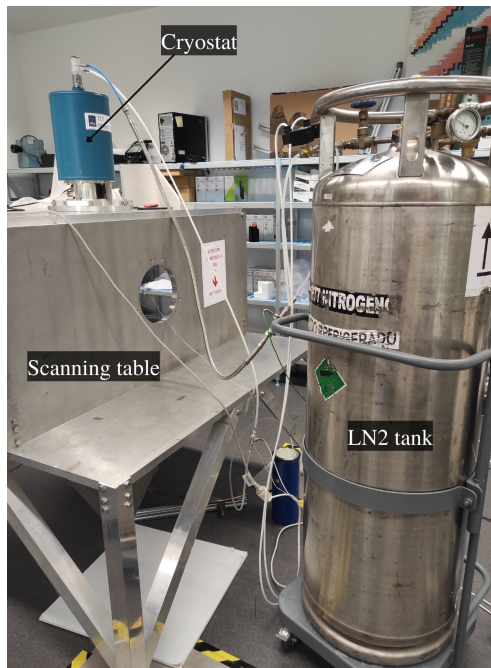
Figure 9: Photograph of the scanning table together with the liquid nitrogen tank connected to the cryostat.

The electronics connected to the detector output are described in the next section.

17

3.2   Measurement electronics

3.2.1   2D scanning

The electronic configuration involved in the measurement process is shown in the following diagram:
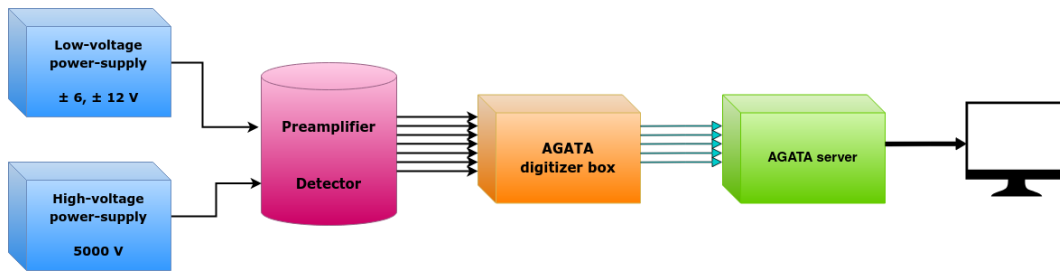
Figure 10: Schematic of the electronic configuration used during the measurements.

First, there is a low-voltage power-supply unit that generates ± 6 V and ± 12 V to power the 37 preamplifiers, one for each segment plus the core. The segment and core preamplifiers are divided into two spatially separated parts, one cold and one hot. The cold stages operate close to the HPGe crystals in the cryostat to optimise noise performance. Furthermore, a good electronic shielding has been developed for the cold preamplifier board to minimise cross-talk effects. As for the hot part, it is at room temperature and is separated from the cold part by a 15 cm wiring inside the vacuum. The core preamplifier provides several particular features: low noise, wide dynamic range in energies, good pulse shape analysis, timing properties, high count capability and an integrated precision pulser [4].

In addition to the low voltage source, a high-voltage power-supply unit is also required to supply 5 kV to the detector. The detector's preamplifier and crystals are located inside the capsule. The output of the detector is connected via seven MDR (Mini Delta Ribbon) cables to the AGATA digitiser. These seven cables transmit the information relating to each of the six vertical sections of the crystal plus the core. In other words, each wire is linked to one side of the detector. As the input of the AGATA digitiser box requires the information of six segments plus the core, the cable of each side is associated with one segment, so that side A corresponds to segment 1, B to segment 2, C to segment 3, etc. The core has its own input.

18
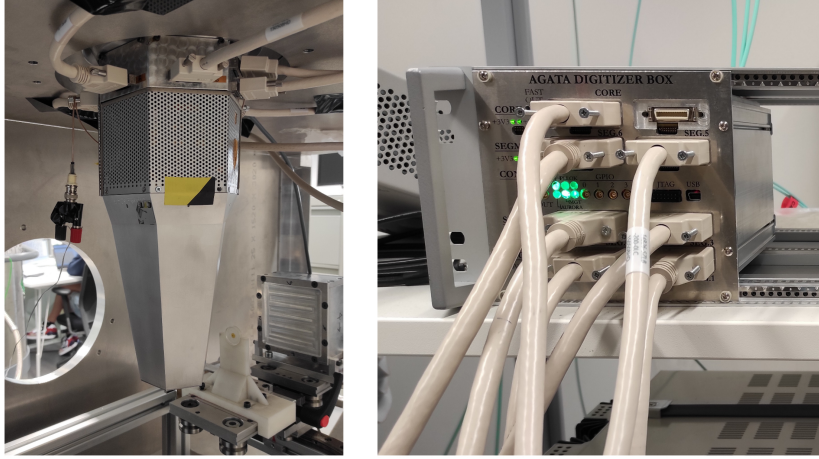
Figure 11: Left: Photograph of the detector on the scanning table. At the top of the detector, it can be observed the MDR cables connecting the output of it to the input of the AGATA digitizer box. Right: Photograph of the AGATA digitizer box with the above mentioned cables. There are seven in total, six of the side segments plus the core.

The output of the AGATA digitizer box contains five ports which are identified, in order, with the core information, segment 1, the control card, segment 2 and 3. These current segments are not related to the previous ones, but are simply used to designate the cables and refer to the readout channels, as they are grouped in such a way that:

· Segment 1: channels 0 to 11

· Segment 2: channels 12 to 23

· Segment 3: channels 24 to 35

In other words, each segment contains the information of a set of channels. As expected, there are 36 data transmission channels, one for each segment of the crystal. For its part, the core has its own cable. Optical fibres are used to connect the five ports to the AGATA server, which are shown in blue in the figure 10.

After passing through the AGATA digitiser box, the information reaches the AGATA server, which sends it to the computer where it is analysed. From the computer, the acquisitions are launched, the measurement conditions are configured and, finally, the required data are obtained from the spectra.

3.2.2   3D scanning

To carry out the 3D scanning of the AGATA capsule, a γ-camera and a ^{22}Na source are used, and the detectors operate in coincidence, as explained in the section 3.5.4. For this reason, information on the γ-camera is given below.

The γ-camera used is composed by four position sensitive scintillation detectors (PSD), which together form a γ-camera with a large field of view, i.e. solid angle, allowing a good spatial resolution to be achieved. Each detector consists of a LYSO scintillator crystal coupled to a pixelated photomultiplier. As for the LYSO crystals, each one has dimensions of 52x52x5 mm^3, so that by joining them together we obtain a single block of 104x104x5 mm^3. Optical grease of the same refractive index as the crystals is placed at the junction between the crystals. In addition, the thickness of the crystals has been chosen to be optimal for the conditions of the experiment we are carrying out. The four crystals are respectively coupled to four pixelated photomultipliers, using optical grease of a refractive index similar to that of the LYSO crystals and the window of the photomultipliers at the junction, to minimise the effect of the medium change on the signal. The photomultipliers are pixelated (PSPMT), Flat Panel Multianode Photomultiplier Tube Assembley type and consist of a matrix of 8x8 pixels. This results in an active area of 49x49 mm^2, although the total size of each device is 52x52 mm^2. Since each photomultiplier has 64 pixels and the γ-camera is made up of four, the γ-camera has a total of 256 readout channels. In addition to the 256 signals from the readout channels, 4 ones are obtained from the anodes, resulting in a total of 260 signals from the γ-camera for each measurement.
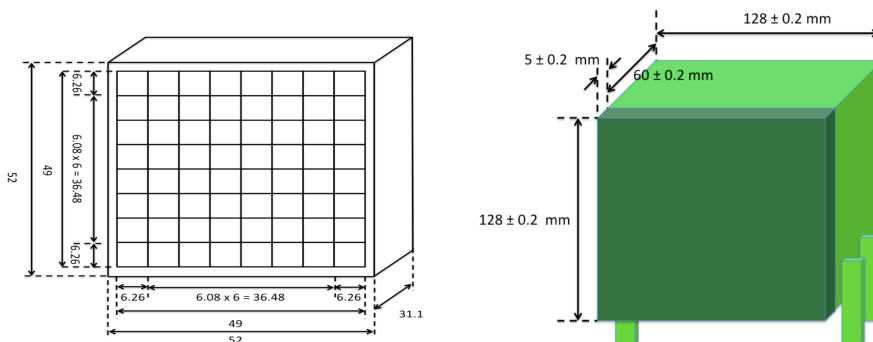
Figure 12: Left: Schematic of Hamamatsu phototube H10966A-100, specifying all its dimensions in mm. Right: Representation of the box encapsulating the γ-camera and its dimensions.
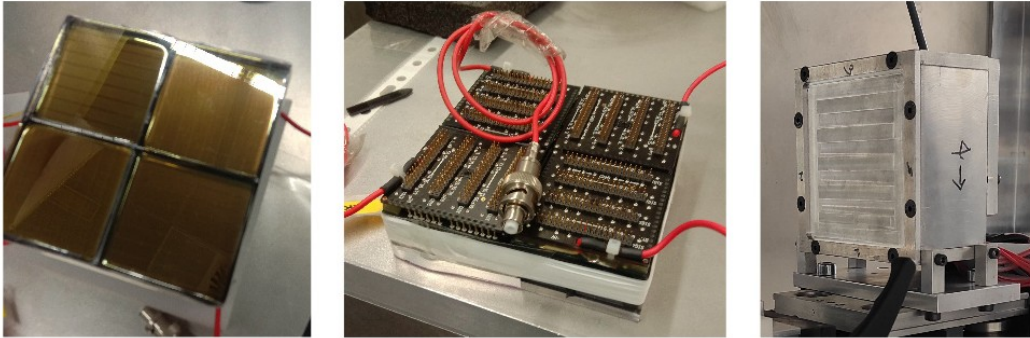
Figure 13: Real images of the γ-camera. Left: the four detectors joined together to form the γ-camera, the LYSO scintillator crystals can be seen. Centre: Output connections of the four photomultiplier tubes. Right: Aluminium box encapsulating the γ-camera with it inside.

To encapsulate the γ-camera, a specially designed and manufactured aluminium box is used, so that all faces are 10 mm thick except those facing the LYSO crystals, which are 5 mm thick, in order to minimise the scattering processes that can compromise the spatial resolution of the system.

The AGATA electronics are similar to the 2D case, also involving the use of the digitizer which is composed of DIGIOPT12s, each of which contains 12 channels.

The most crucial part of the 3D scanning electronics is the logic circuit to establish the coincidences. A schematic of this circuit is attached below:
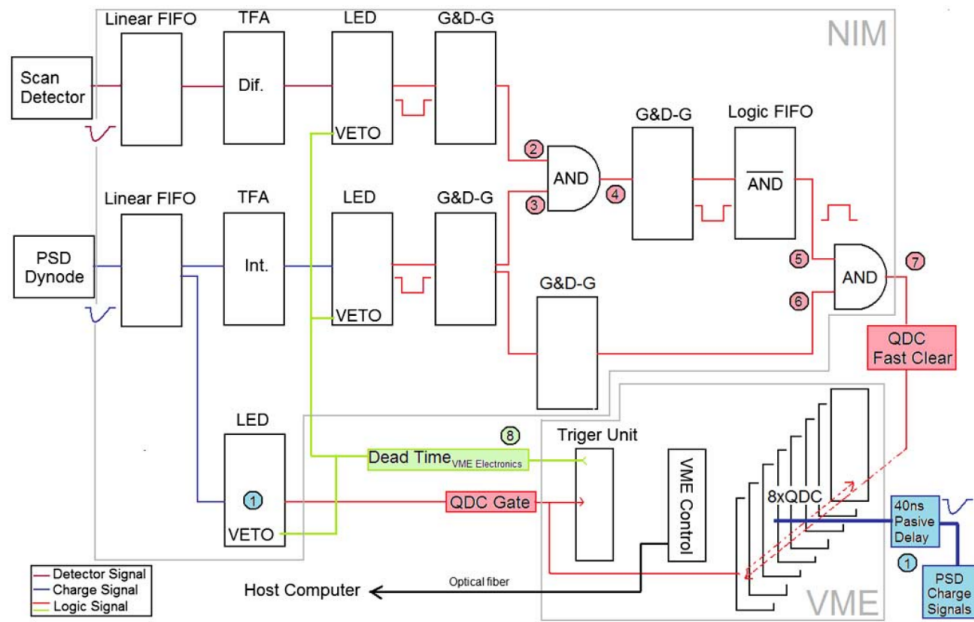
Figure 14: Diagram of the logic circuit for launching the acquisition electronics.

During measurement, two processes run in parallel: on the one hand, the acquisition of the signals from the γ-camera and the HPGe detector and, on the other hand, the logic that leads to discerning whether an event has occurred in coincidence or not. VME technology is used to acquire the signals, while all the coincidence logic is incorporated in the NIM crate.

The signals of charge coming out of the dynodes of each PSD (γ-camera) are sent to a FIFO (Fan In/Fan Out) module which duplicates the signal and allows one of them to be sent to the coincidence logic circuit and the other to the acquisition electronics. The signal destined for the acquisition electronics is fed into an LED (Leading Edge Discriminator), which is a module that is used to trigger a signal when the incoming one exceeds a certain threshold, i.e. it is used to mark the start of a pulse when the signal reaches a certain voltage amplitude threshold. The LED generates a digital logic signal from an analogue one when it exceeds a preset threshold. The digital output of the LED is sent to the QDCs, where it is used as a logic gate that indicates to these modules when to start the integration stage and subsequent digitisation of the signals of each of the pixels of the γ-camera. Actually, there are eight QDC (Charge to Digital Converter) modules, each with 32 channel inputs, that integrate and then digitise the charge signals of the PSDs, on receiving the start indicator from the LED. The signal acquisition takes place in the QDCs, which work in parallel, simultaneously, to the coincidence logic

process that will be described below [6].

Among all the events that trigger the acquisition in the QDC modules, it is necessary to determine which of them are really valid, that is, which have occurred in time coincidence between the AGATA detector and the γ-camera. Since, as mentioned above, the QDCs work in parallel and acquire the signals coming from the PSDs while the logic that decides whether the event occurs in coincidence is being carried out, the strategy followed is to consider all the possible events and delete those that do not occur in coincidence. That is, during acquisition, all possible events are taken into account and then those that do not occur in coincidence are removed. Instead of selecting valid events, i.e. coincidence events, invalid ones are eliminated, thanks to the Fast Clear function of the DQC. When an event is identified as invalid, the integration in the QDCs is interrupted and a waiting state launched until the next event arrives. To identify the events that do not occur in coincidence, we employ the electronics which are schematized in the figure 14. The signal from the AGATA detector is first fed into a FIFO that duplicates it. One of the outputs is routed to a differentiating TFA (Timing Filter Amplifier) and the other is fed into a secondary circuit which will be discussed later. The differentiating effect of the TFA is used to change the signal from having two LED triggers to a single one. After TFA, the signal is routed to a LED discriminator, which is triggered when the signal exceeds a certain threshold in voltage amplitude and thus serves to determine the presence of a pulse of interest. The LED discriminators are connected to a VETO which avoids triggers when the VME acquisition system is busy. Then, the digital signal is directed to a G&D-G (Gate & Delay Generator), that is used to align two signals in time, those of the two detectors. The γ-camera uses the same electronic module scheme, except for the behaviour of the TFA, which in this case is an integrator and reduces the noise of the signal. Finally, both signals are sent to an AND [3] gate and pass through a succession of logic gates which determine coincidence events, leading to the next result:

· If the event is in coincidence: the Fast Clear of the QDC is not activated and the event is not deleted, it is saved.

· If the event is not in coincidence: the Fast Clear of the QDC is triggered and the event is removed.

---

[3]The AND logic gate behaves as follows: Only when both inputs are true (1), the output will also be true (1). If one of the two inputs is not true (1), then the output will be false (0). For the output to be true (1) both inputs must also be true (1); otherwise it will be false (0). Its mathematical expression is the product: $Output = Input_1 \cdot Input_2$.

23

As the system is composed of the sequence AND gate - inverter FIFO[4] - AND gate - Fast Clear function, the following possibilities are available:

γ-camera	HPGe detector	AND	NOT	AND	Fast Clear
0	0	0	1	0	
0	1	0	1	0	
1	0	0	1	1	True Operates Deletes the acquisition
1	1	1	0	0	False Does not operate Stores the acquisition

Table 3: Truth table through the logic gates of the circuit and the performance of the Fast Clear as a function of the input signals.

It is important to remember that the first AND gate receives as inputs the signals from the γ-camera and the HPGe detector, while the second AND gate takes as inputs the output of the inverting FIFO and the γ-camera signal. In the detectors, 1 (true) is identified as the generation of a signal for having detected a particle, while 0 (false) is understood as the detector not having been triggered. For this reason, the events in coincidence are those that correspond to the last line of the table 3. The acquisition is only initiated when an event is registered in the γ-camera (PSD), so it is only of interest to save or delete this data when this detector is triggered. That is why when the γ-camera does not register any pulse (lines 1 and 2 of the table 3) there is no sense in using Fast Clear, since it cannot stop an acquisition that has not been previously started.

In summary, the electronics scheme is designed in such a way that the NIM part is dedicated to analyse the coincidences, so that it deletes invalid events and saves valid ones.

The question is, why do we operate with the two processes working simultaneously, in parallel? Why do we delete the events that are not in coincidence instead of waiting to find out which ones are valid and select them? The reason is it is necessary to start the integration phase as quickly as possible, otherwise we would have to introduce a passive delay in the 256

---

[4]The logic FIFO is used to invert the signal, like a NOT logic gate. That is, true signals (1) are converted to false ones (0), and vice versa.

Figure 15: Photographs of the experimental electronic setup. Left: NIM and VME racks where the electronic modules are placed and the cables that establish the connections between them. Right: Signal generator used to create the ramp.

signals coming from the γ-camera, which would lead to a significant loss of quality.

As discussed above, one of the outputs of the FIFO connected to the HPGe detector is routed to the logic circuit while another is sent to a secondary circuit. In this secondary circuit, the output of the FIFO is fed into a second FIFO together with signals from a ramp and other elements, such as a logic signal and a trigger. The output of the second FIFO is split into two lines, the first goes to the STRUCK while the second is fed into a third FIFO. This module is used to extract a signal similar to the input one and its inverse. In other words, the inverting function of the FIFO is used on one of the lines, thus obtaining an unaltered signal and its inverse at the output. These signals are routed to pins 11P and 11N of a PCB, and finally to the digitizer. A PCB board is also used to split the core signal.

The ramp is a signal that is introduced through a ramp generator and is employed to know the temporal start of a measurement, in order to be able to adjust the signals in time. That is, the ramp is used as a time meter, to mark a start and to be able to correlate the signals.

3.3   Radioactive sources

During the scanning procedure four γ-ray sources are used: ^{241}Am, ^{60}Co, ^{137}Cs and ^{22}Na.

The ^{241}Am is a radionuclide with a half-life of 13.652 $\cdot 10^9$ s, equivalent to 432.6 years, which decays via α to ^{237}Np. The latter presents a complex system of decay levels, although its main desexcitation takes place through the emission of a γ ray of 59.5409 keV, with an intensity of 35.92%. That is, the ^{241}Am can be considered as a source of 59.5409 keV γ rays. As these are very low energy rays, the ^{241}Am is used to characterise the nearest surface of the crystal, i.e. the bottom one. The ^{241}Am rays penetrate little into the detector since they deposit all their energy at a shallow depth. That is why it is employed to define the edges of the segments in the lowest ring, the one closest to the source, performing a first general scan and then a more exhaustive one.

The ^{137}Cs has a half-life of 948.3 $\cdot 10^6$ s, i.e. 30.05 years, and decays β^- to ^{137}Ba. The main ^{137}Ba γ emission occurs at 661.657 keV, with a probability of 84.99%. Therefore, ^{137}Cs appears as an emitting source of γ rays of energy 661.657 keV.

The ^{60}Co is a radionuclide of half-life 166.340 $\cdot 10^6$ s, i.e. 5.2711 years, which decays to ^{60}Ni. The ^{60}Ni has two γ cascade emissions, that is, the second emission is conditioned by the first one. The two emissions are correlated and, although one occurs immediately after the other, as the process is very fast the rays are considered to be emitted at the same time. The first γ ray has an energy of 1173.228 keV and an intensity of 99.85%, while the second ray has an energy of 1332.492 keV with 99.9826%.

The ^{60}Co and ^{137}Cs sources are used to characterise the crystal in volume. As both radionuclides emit more energetic γ's than ^{241}Am, they penetrate deeper into the crystal and allow a study in volume to be performed. Since ^{60}Co and ^{137}Cs γ's rays reach almost all the segments, i.e. all the rings, they are used to determine the position of the hole and its inclination.

The ^{22}Na is a radionuclide with a half-life of 82.140 $\cdot 10^6$ s, equivalent to 2.6029 years, which decays via β^+ to ^{22}Ne. The ^{22}Ne is desexcited by emitting a γ ray of energy 1274.577 keV with an intensity of 99.94%. As already mentioned, the ^{22}Na is a β^+ source, i.e. it emits positrons. These positrons, which come out practically at rest, their kinetic energy is almost

zero, annihilate with the electrons of the medium, generating two γ rays of energy 511 keV. By the conservation principles of energy and momentum, the two 511 keV γ rays produced as a consequence of the annihilation are emitted in the same direction and opposite orientation, that is, forming an angle of 180º between them. It is precisely this property, the 180° emission, which is the basis of the 3D scanning. Therefore, for the 3D scan a source of ^{22}Na is used, which provides collineal γ rays emitted in opposite orientations, necessary for the trajectory reconstruction.
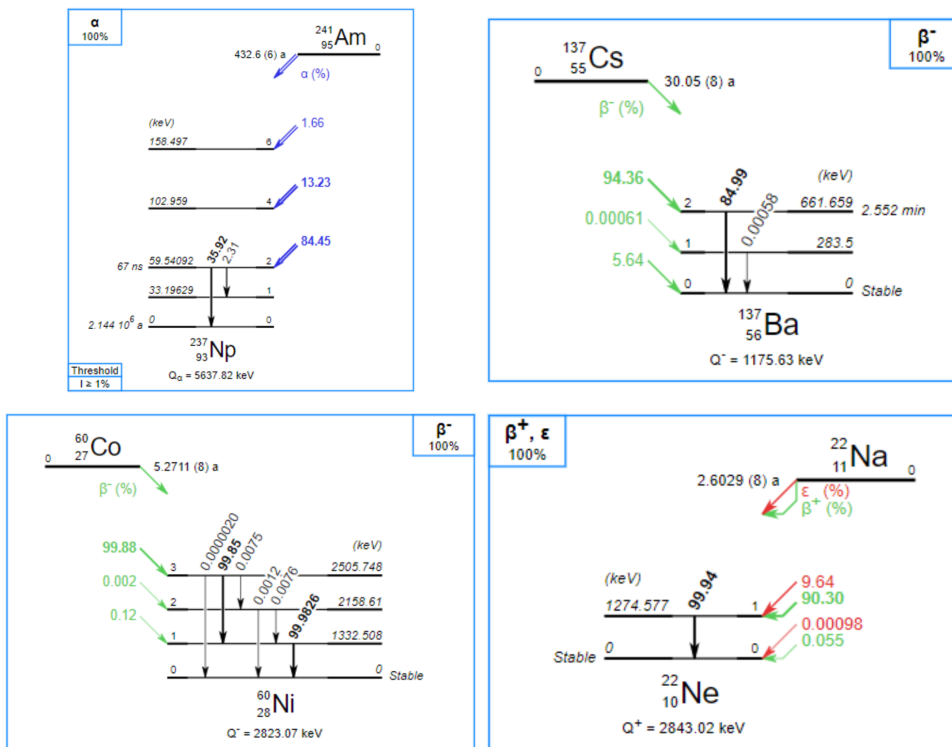
Figure 16: Decay schemes of the sources used for characterisation.

3.4   Process before measurements

In order for the HPGe crystals to operate properly, they must be kept always at very low temperatures. For this reason, before starting the measurements, a preliminary process must be carried out in which the capsule is conditioned to its operating point. This process consists of the following steps:

· First, vacuum is created in the cryostat by connecting it to a vacuum pump. At the beginning, the process must be very slow, so that the pressure difference is not too great and can damage the cryostat devices. For this reason, the vacuum procedure is carried out in two stages. The pump is connected to the cryostat through a device containing a valve, and the first stage consists of vacuuming the connecting tube, plunger, up to the valve. In other words, the vacuum is not created directly in the cryostat, but first in the connecting tube up to the valve. When the vacuum pump is switched on, the pressure drops very quickly. Over time, however, the process slows down, as it becomes more and more difficult to reduce the pressure. When the pressure is of the order of 10^{-6} mbar, the valve is opened so that the vacuum pump and the cryostat are directly connected.
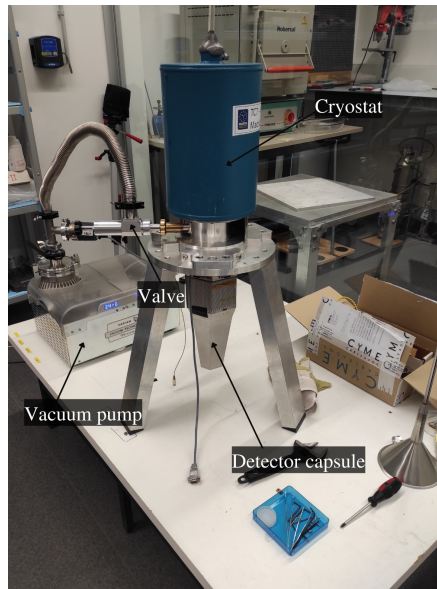
Figure 17: Photograph of the A005 capsule with the cryostat connected to the vacuum pump.

As before, the pressure decreases very quickly at the beginning. In order to avoid damage to the cryostat components, the pressure must

be equalised slowly. However, as time passes and the pressure becomes lower, it becomes more and more difficult to reduce it, as it stabilises and decreases more slowly. When the pressure is of the order of 10^{-6} mbar, we start filling the cryostat with liquid nitrogen (LN$_2$) to cool it down.

· Without disconnecting the vacuum pump, we start to cool the cryostat with liquid nitrogen. The refilling is done manually, following a pre-established protocol. In this situation, it is important to pay attention to two magnitudes: the temperature in the cryostat (which is calculated by measuring the resistance) and the vacuum level, pressure. When the pressure is of the order of 10^{-7} mbar, the vacuum valve is closed and the pump is switched off.

· The capsule is moved to the scanning table and placed in the hole at the top. The cryostat is then connected to the liquid nitrogen tank through the automatic refilling system. It is necessary that the capsule is kept at cryogenic temperatures during the entire measurement process, otherwise components may be damaged and the detector will not operate correctly.

· The capsule, i.e. the detector, should be as vertical as possible, with its axis perpendicular to the plane of the table. To adjust the inclination, and to achieve the greatest verticality with respect to the table, a level is used while manipulating the micrometric screws at the base of the hole on which the capsule rests.

· Finally, all the electronics are connected and the detector is powered with a high voltage of 5000 V. During this power supply process, it is necessary to check the signal of the core preamplifier in the oscilloscope.

3.5   Experimental procedure

Before explaining in detail the measurement process of each scan and its subsequent analysis, two basic criteria that mark the quality of a scan are presented:

· Firstly, the spatial distance between two successive points. The closer the measurements are to each other, the better characterised that space will be, because finer details can be achieved.

· The measurement acquisition time at each point. As the measurement time increases, the statistics of the results improve so they become more reliable.

However, we have to take into account that the project has a defined duration, so a reasonable compromise has to be made between the two parameters above and the total characterisation time.

The procedure followed for scanning and the approach to data analysis is detailed below.

3.5.1   General horizontal 2D scanning

First, a general horizontal scan is carried out with a source of ^{241}Am. This initial scan allows to obtain a first reconstruction of the segments composing the lower ring, i.e. the number 1. The source is placed in different positions within a grid, fixing a value on the x-axis and varying the y-axis, and vice versa, sampling the whole space. As for the technical details, a 3 mm diameter broad collimator is used, and the measurements are taken 1 cm by 1 cm, i.e. the scanning is performed in a grid of 1 cm x 1 cm. In this way, it is possible to get a first idea of the structure of the lower ring.

To this end, for each measurement, i.e. position, a spectrum of the radiation recorded by each segment and the core is obtained. The spectra corresponding to the segments that make up the lower ring are the only taken into account, and, for each of them, the peak due to ^{241}Am is considered and its area is calculated, through the spectra analysis programme TkT. In a data storage software, such as Excel, the values of the peak areas of each segment are collected. In other words, for each measurement, we note down the position (x and y coordinates with respect to the reference system defined on the scanning table), the acquisition time and the area of the peak in each segment, 6 in total. For a correct analysis, the data that is actually used is the peak area divided by the measurement time, which is related to the number of counts recorded by each segment in the time unit. For each segment, these values are plotted on the z-axis versus the position on the x- and y-axis. Thus, we obtain a 3D diagram that provides a first idea of the position of the segment edges. However, the reconstruction is very rough, with little detail, so a more exhaustive scan is then carried out to determine the position of the segment edges more accurately.

As mentioned above, in this case, the analysis strategy is very simple and consists of the representation of the number of counts per unit of time (z-axis) versus the position (x and y axes) for each segment.

3.5.2 Specific horizontal 2D scanning for the determination of transverse segment edges

After the previous scan, we have a first idea of the location of segment edges, but with little precision. For this reason, a more exhaustive, detailed study is carried out in these regions of interest.

Segment boundaries are understood as axes that separate one segment from another. That is why, to characterise them, measurements are taken on both sides of the edges, so that what is really being analysed is the counting in the adjacent segments. For each boundary, a series of imaginary lines are drawn, parallel to the x or y-axis, as appropriate, which intersect the border in question. Actually, measurements are taken along four of these lines for each boundary, with a finer collimator of 1 mm diameter. Several measurements are made on these lines with 1 mm separation, step, on both sides of the edge, i.e. on the segments defining it. A diagram of the measurement positions is included below for a better understanding:
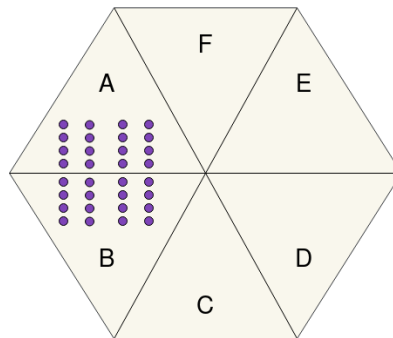
Figure 18: Example of measurements to determine the border between segments A-B. The purple dots define the measurement positions.

As can be observed in figure 18, measurements are taken on both sides of the border, on each segment of interest. At each measurement line, the x-axis or y-axis is fixed for convenience and to facilitate data analysis. Results are expected to be of the form:
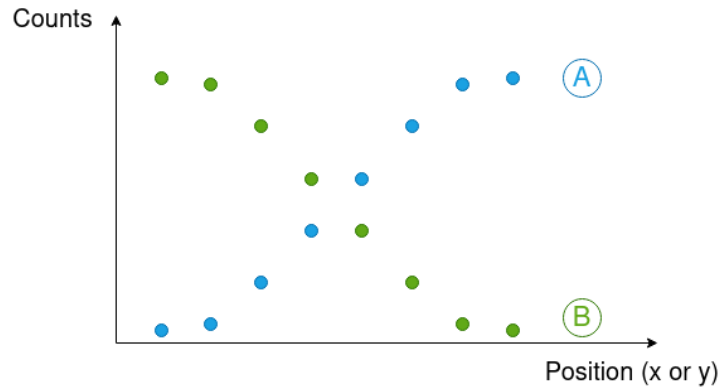
Figure 19: Representation of the results obtained in segments A and B (example) when measuring at different positions on an imaginary line on which the x or y-axis is fixed.

When the collimated beam is incident on one segment, the count is very relevant on this segment and practically null on the rest. However, when the source is placed under an edge, the count on the adjacent segments should be equal in principle. In fact, we take advantage of this result to locate the edge, i.e. when two segments register practically the same counting, it is because the beam is incident on their common edge. By plotting the results of each line of measurements we obtain graphs like figure 19. The next step is to consider the points that lie in the central area and to perform a linear fit from them (one for each segment). This gives the equations of two lines, whose intersection defines a point. This point belongs to the border between segments. Thus, from each line of measurements we get a point that belongs to the border. Since the scan is performed on four lines for each boundary, four points which in principle belong to this edge are obtained. Finally, by fitting them to a straight line, the equation defining the boundary is determined. The same procedure is followed for all six edges and thus they are identified experimentally.

3.5.3   Specific horizontal 2D scanning for the location of the central hole and its inclination

Through this scan, it is intended to determine the real position of the central hole and its inclination with respect to the vertical axis. Actually, it is interesting to find the tilt of the hole in order to know the inclination of the detector. The aim is to correct its orientation in case it is tilted at a certain

angle. For this scanning, the ^{241}Am source is replaced by ^{60}Co and ^{137}Cs, which have more energetic γ-rays that penetrate the detection material.

The strategy used to locate the hole and know its inclination with respect to the vertical axis is as follows:

Measurements are taken along two lines, one parallel to the x-axis and the other to the y-axis, varying only one of the two coordinates. In addition, these lines are chosen so that they pass through the centre of the crystal (the position is known from previous scans). Although a small number of measurements are taken, this is sufficient because the importance of this scan lies in finding out whether the detector is tilted or not, and, in second place, the position of the hole. The main objective is to discover the inclination of the crystal with respect to the vertical axis and for this purpose the taken measurements are enough. Furthermore, it is known from the manufacturing documents that the hole has a diameter of 10 mm. Therefore, a series of measurements are taken on two lines parallel to the x and y-axes, as shown in the following graph:
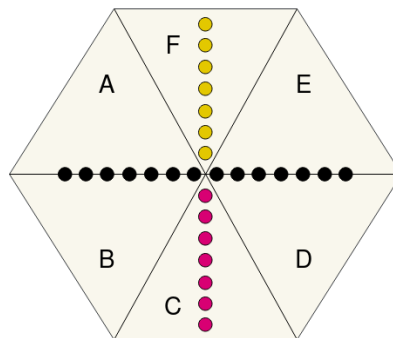
Figure 20: Example of measurements to determine the central hole position and its inclination.

To analyse the data obtained from the measurements, the results of each ring are studied separately. In other words, a study is carried out to locate the position of the hole in each slice. The idea is to determine the location of the central hole in each ring and thus deduce whether the detector is tilted or not. If the hole appears in the same position in all the rings, the detector will be perfectly aligned with the vertical axis, whereas if the position varies from one slice to another, it will be concluded that the detector is tilted, figure 21.
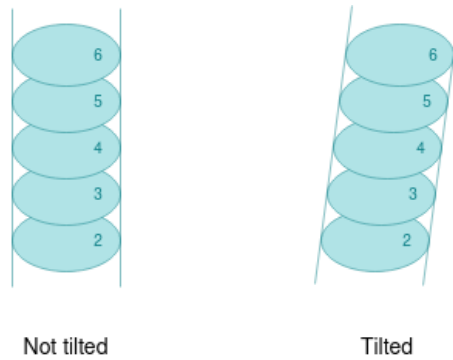
Figure 21: Determination of the detector's inclination with respect to the vertical axis as a function of the position of the hole in each slice. The hole extends from segment no. 2 to segment no. 6, then the first segment, the lower one, does not have a hole in it.

In order to know the location of the hole in each ring, it is important to take into account that when the beam hits it, the counting decreases very significantly in the segments, being practically null, since those γ-rays are not detected in any crystal. This is the basis for the analysis of the data. For each slice, on the one hand, the count in three segments is summed and, on the other hand, the count in the other three segments. It is necessary to take the sum of three segments because the collimator is not thick enough and some γ-rays are expected to escape and produce counts in nearby segments. The segments are selected to group the three that remain on one side of the hole and those that remain on the other part, following the line of measurements. That is, along this line, there are three segments that are closer to the measurements on one side and three that are closer to the other measurement region. In the figure 20 it can be observed that the segments A, E and F are closer to the measurements on the upper part while the segments B, C and D are closer to the measurements on the bottom side. In the data analysis, for each ring, we add the count of the A, E and F segments, on one side, and the counting of B, C and D segments on the other. Plotting the results obtained from these sums against the position (x or y coordinate), we obtain graphs of the form:
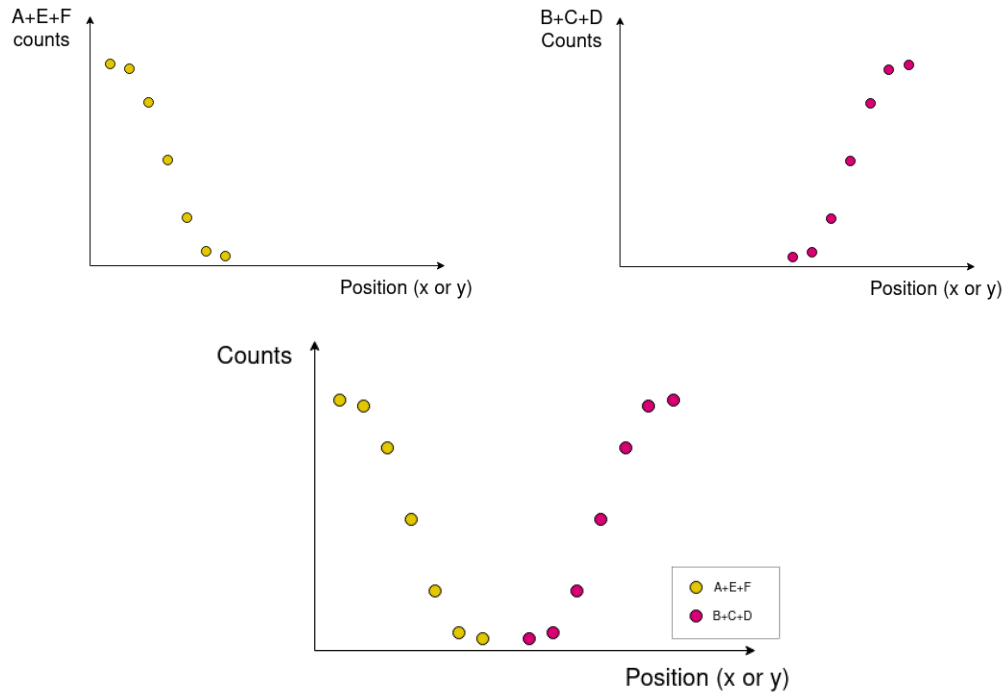
Figure 22: Representation of the expected results to locate the hole: sum of segments A+E+F (left), B+C+D (right), combination (down).

The method of sum of counts between three segments allows to smooth the results and to obtain curves that better reconstruct for the expected behaviour. The combination of the results obtained on one side and on the other allows the central hole to be located. It should be noted that the statistics of the measurements are rather poor, so it is necessary to carry out a correct data processing. In other words, the raw results are filtered and those that deviate from the general behaviour are eliminated, selecting only those that are of interest. In this way, more physically meaningful results are achieved. The deep in the curve is linked to the hole.

As mentioned above, we are really interested in knowing the inclination of the detector with respect to the vertical axis, and for this purpose we study the inclination of the hole. To determine the inclination of the hole, we compare the position of the centre point of it in each ring, according to the criteria shown in the figure 21. That is, we assess whether the centre of the hole, the midpoint, is in the same location in all the slices or whether it varies from one slice to another. For this reason, it is necessary to find the midpoint of each ring, following the next procedure: for each slice, two linear fits are made with the points of the results that are part of the hole

boundaries, one for each boundary. These two lines intersect at a point whose coordinate (x or y) corresponds to the midpoint sought. One analysis is performed for the determination of the x-position and one for the y-position, for each ring. This gives the location of the centre of the hole in each slice, denoted as (x_i,y_i). If $x_2 = x_3 = x_4 = x_5 = x_6$, the detector will be aligned in the x-coordinate; if in addition $y_2 = y_3 = y_4 = y_5 = y_6$, it will also be aligned in the y-coordinate, so it will be in a perfectly vertical position. Otherwise, the detector will be tilted.

3.5.4   3D scanning

The 3D scanning is the most important part of the capsule characterization process, since it consists of an active collimation analysis method that stands out from other more mechanical procedures carried out by other research groups within the AGATA collaboration.

It is based on the combination of two fundamental ideas:

· When a γ ray interacts in the active volume of the detector, it generates a charge signal in the segment where it has been detected but also in the adjacent segments, which are affected by this interaction. In other words, induced signals appear in the contiguous segments to the one where the detection occurred depending on the interaction position. The induced charge in each adjoining segment is proportional to the distance between the interaction point and the segment where the induced pulse appears. That is why each position generates a set of characteristic pulse shapes in the segment where the detection occurs and in the contiguous ones. This is the key idea of the 3D scanning characterisation: Each interaction position in the detector is characterised by the shape of the pulses in the segment where it occurs and in the adjacent ones. For this reason, the ultimate goal of the characterisation is to know the electric response corresponding to each interaction position, and to collect this information in a database. For this purpose, the Pulse Shape Analysis (PSA) technique is used. The scan is performed from 2 different detector-source-γ-camera system configurations, because if the set of pulse shapes is the same from two different directions, it is because it is the same interaction position. In addition, the PSA technique allows to determine the energy deposited in the detector by the photon through the integration of all the charge signals [6].
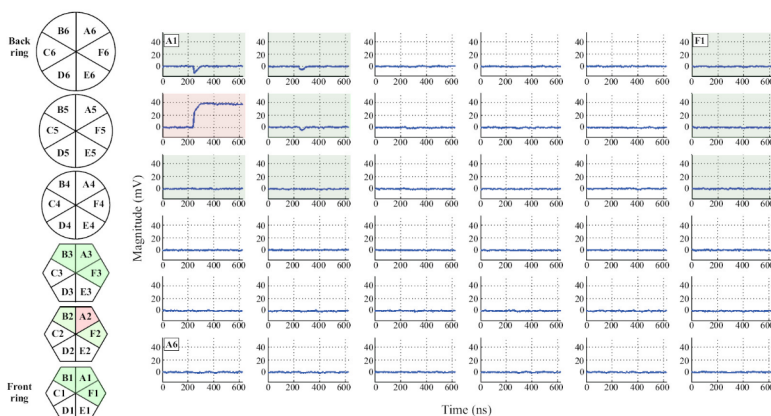
Figure 23: Representation of the output of preamplifiers when a γ ray interacts in one segment (red) and generates induced signals in adjacent ones (green).

· The second important idea is the reconstruction of the position through tracking algorithms. As mentioned above, the source used for the 3D scanning is ^{22}Na, which is a β^+ emitter. This source allows the generation of two collinear photons of energy 511 keV after e^-e^+ annihilation. These γ rays are emitted at 180°, i.e. in the same direction but in opposite orientation. For this reason, when one of the photons reaches the AGATA detector, the other one is recorded in the γ-camera. Therefore, this property of ^{22}Na is used to discover the interaction position of the γ ray in the HPGe crystal once the detection position in the γ-camera is known. That is, knowing the location of the source and the position of the interaction in the γ-camera, it is possible to reconstruct the photon trajectory and to determine the interaction point of the other γ in the AGATA detector, as all of them should be in the same line. That is why the measurements in the 3D scan are carried out in coincidence between the two detectors. This mechanical position is related to the set of pulses obtained in the different segments, as explained above, and thus the relationship between the position and the pulse shapes is established. The reconstruction of the trajectory using the γ-camera and the source allows the interaction position in the AGATA crystal to be determined and this point is linked to the corresponding set of pulse shapes in the segments.

To this aim we use SALSA (SAlamanca Lyso-based Scanning Array) which is the characterisation system developed in Salamanca to determine the electrical response of HPGe detectors with segmented contacts. It is

based on coincidence detection between a position-sensitive detector (PSD), such as a γ-camera, and the detector to be scanned, and the use of pulse shape analysis techniques.

The mechanics of SALSA consists of a structure that allows all the elements, source and detectors, to be held together under a common frame of reference. It is composed of an arm containing the support for the source and the γ-camera inside a circular circuit. This circuit allows the arm to rotate around the axis of the AGATA capsule and to move from the S1 to the S2 position, as illustrated in the figure 24. In addition, the design of the mechanical arm is such that the distance between the different elements can be adjusted.
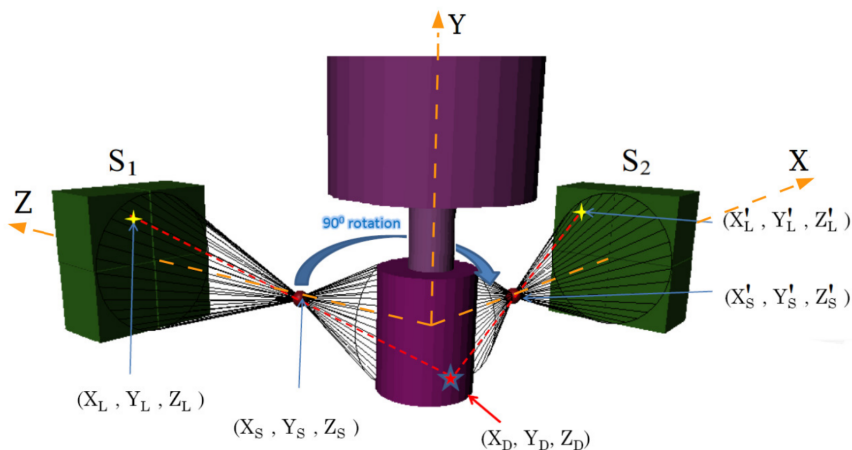
Figure 24: Schematic of the SALSA mechanics, with the γ-camera (green) and the ^{22}Na source (red) arranged with respect to the HPGe detector (purple). The two scanning positions, S1 and S2, are depicted and the notation used is included.

To find the interaction position of the photon inside the detector, it is possible to derive a set of equations that give the coordinates of that point with respect to the common frame of reference. For this purpose, we use the line joining the photon interaction positions in the γ-camera and the germanium crystal and the location of the source. The three elements have to be aligned since the γ rays are collinear. The position reconstruction algorithm uses a series of equations that can be derived involving several reference frames, for the different elements, and establishing relationships between them. In this way it is possible to reach to the following equations:

$$X_D = \frac{\frac{X_S(Z_L-Z_S)}{(X_L-X_S)} - Z_S + Z'_S - \frac{X'_S(Z'_L-Z'_S)}{(X'_L-X'_S)}}{\frac{(Z_L-Z_S)}{(X_L-X_S)} - \frac{(Z'_L-Z'_S)}{(X'_L-X'_S)}} \tag{1}$$

$$Y_D = \begin{cases} \frac{(Z_D-Z_S)}{(Z_L-Z_S)}\left(Y_L - Y_S\right) + Y_S & (Recta1) \\ \frac{(Z_D-Z'_S)}{(Z'_L-Z'_S)}\left(Y'_L - Y'_S\right) + Y'_S & (Recta2) \end{cases} \tag{2}$$

$$Z_D = \frac{(X_D - X_S)}{(X_L - X_S)}(Z_L - Z_S) + Z_S \tag{3}$$

Where (X_D, Y_D, Z_D) are the sought coordinates, i.e. the interaction position of the γ ray inside the HPGe crystal, (X_L, Y_L, Z_L) refers to the interaction position of the other γ ray in the γ-camera, and (X_S, Y_S, Z_S) corresponds to the annihilation point where the γ rays were generated in the ^{22}Na source. All coordinates are referenced to the global frame of reference centred on the HPGe crystal. The prime coordinates (') designate the same positions but from the S2 configuration. It can be seen that we obtain expressions for the coordinates X_D and Z_D, and a geometrical condition for Y_D, which allows to know if the trajectories of the S1 and S2 configurations intersect at a point.

The ultimate goal of the AGATA spectrometry is the trajectory-based position reconstruction. The aim is to develop position-sensitive detectors with high resolution and low segmentation. To achieve this goal, a pulse shape database must be constructed as complete as possible. This database must contain information about the electrical response of the detector for each photon interaction position into the crystal. That is, knowing the detector response, in terms of pulses, the database should provide the photon interaction position. For this reason, it is essential to work on the improvement of this pulse database, since it conditions the determination of the interaction position of the photon in the crystal and, consequently, the resolution, which is a key magnitude in the reconstruction of the trajectory. In addition, performing the measurements in time coincidence between the detector to be characterised and the γ-camera allows the contribution of the intrinsic activity of the LYSO crystal, its own emissions, to be very considerably reduced.

To summarise, the main ideas to highlight of the 3D scanning are the following: The measurements are carried out with the detectors operating in coincidence, taking advantage of the collinearity of the photons produced as a consequence of the ^{22}Na source. For this reason, no external elements, such as collimators, are needed to focus the beam, as the method used provides

active collimation, i.e. the photons themselves define the direction and positions of interaction. The combination of this technique with Pulse Shape Analysis (PSA) process makes it possible to obtain a very well-defined 3D image employing only two scanning positions.

3.6 Analysis software

In order to analyse the spectra and obtain the necessary information from them we use the computer software TkT. This programme allows us to analyse simultaneously the 37 spectra obtained from each measurement, 36 of the segments plus the core. When opening a file, it displays the 37 spectra in two visualisation modes, grid or vertical. As mentioned above, the relevant information obtained from each spectrum is the area of the peak of interest. For this reason, the programme allows us to select each spectrum individually, carry out its calibration in energies and perform a Gaussian fit. From the Gaussian fit of each peak, we get, among other data, its area.
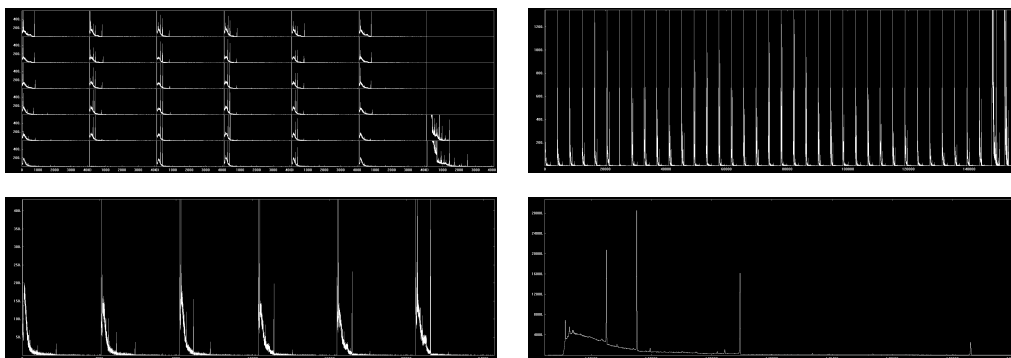
Figure 25: Screenshots of the TkT software. Top left: set of spectra of a measurement displayed in a grid. Top right: spectra displayed vertically, in a row. Bottom left: spectra of the segments belonging to the first ring. Bottom right: example of a spectrum recorded by a segment.

For the representation of the results we use the software Origin. This programme allows a large amount of data to be represented in different forms, such as 2D, 3D graphics, etc. It also contains an important number of tools that are useful for the analysis of the results and the graphs obtained.

3.7   Geant4 simulation

To assess the validity of the experimental results, a simulation that reproduces the laboratory structure during the 3D scanning is implemented with Geant4 software.
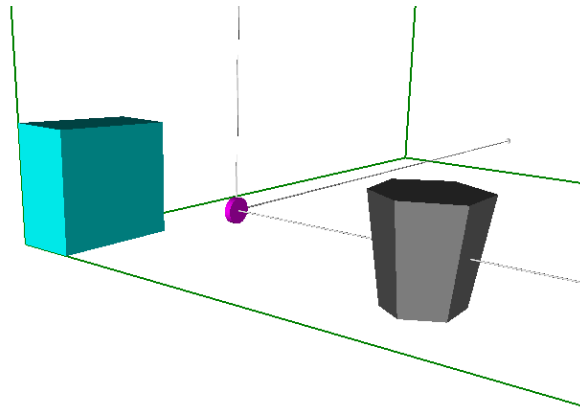
Figure 26: Visualization of the simulated experimental setup using Geant4 software. The AGATA capsule is shown in grey, the ancillary detector corresponding to the γ-camera in cyan, and the ^{22}Na source encapsulation in magenta.

Geant4 (for GEometry And Tracking) is a computer toolkit that allows simulating different physical elements, such as detectors and particles, as well as the processes they experience in their interaction with matter. This software is composed of a set of C++ classes that use Monte Carlo methods for their execution. One of the main advantages offered by this programme is the tracking of each particle through the different defined volumes.

In order to reconstruct the experimental structure, three main volumes are included in the simulation. The first one, corresponding to the AGATA capsule, which involves different files such as solid, clust, euler or walls, where the following geometric information is included in each of them:

- · Solid: the geometry of a single AGATA crystal is defined, in this case, A-type.

- · Clust: the crystal is positioned within a cluster, using translations and rotations through euler angles.

- · Euler: the cluster with the crystal is established into the world.

41

· Walls: the walls of the capsule covering the crystal are defined with respect to the reference frame of the cluster.
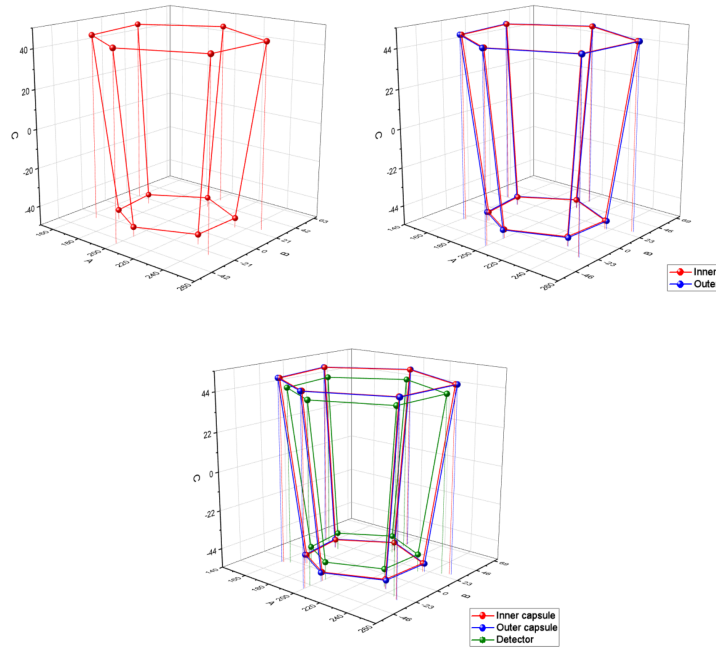
Figure 27: Reconstruction of the AGATA capsule through the definition of its vertices, represented with the Origin software. Top left: representation of the HPGe crystal. In addition to the represented vertices, we actually also simulate a cylinder in the upper part of the crystal whose intersection with the hexagonal pyramid trunk results in the real geometry of the detector. Top right: Reconstruction of the walls of the shell. We show the vertices of the side walls, with the inner and outer surfaces. Bottom: Representation of the whole set, with the vertices that generate the crystal and the walls of the encapsulation. Dimensions are in mm.

It should be taken into account that both the geometry of the crystal and the geometry of the coating capsule are defined by a set of elements, such as surfaces, cylinders, etc. As these ones make use of the vertices that limit them, ultimately, what is really registered are the points, vertices, that define the surfaces of the crystal and the capsule.

On the other hand, we use another set of files to incorporate the volume referred to the γ-camera, which is included in the simulation as an ancillary detector.

Finally, the ^{22}Na source is simulated using the gps (general particle source) tool. Its data are added in the macro that allows the simulation to be run.

In addition to the files relating to the geometry of the volumes, we also require files that include information on the materials that make up the detectors, the physical processes and particles involved, the generation of events etc.

After compiling and executing the AGATA code, the results are fed into a programme for analysis.

Actually, when the simulation is run, a set of files is generated, including one that collects information about the detection of photons in the detectors. This file stores data on the γ-ray interactions in the detectors, such as the positions at which they occur, the energy deposited in each of them or the segment triggered in each case. The mentioned file is fed as input to a second program, which analyses the previous raw data. The code is written in a way that allows the study of interesting properties to be applied in the experimental process, i.e. it provides an idea of what would be expected in the real experiment. Relevant aspects to be analysed include the following:

· The efficiency of the system in coincidence. The number of photons that are registered in temporal coincidence in the two detectors is studied in comparison with the number of photons produced by the source. In terms of simulation, it is understood that two photons are detected in coincidence if they refer to the same event. It is also possible to determine the efficiency of the detectors individually, without introducing the coincidence condition. Knowing the efficiency of the system, it is possible to estimate the time needed for experimental measurements.

· The distribution of interactions between the different segments. The aim is to determine whether the photon interactions are equally spread across all segments of the AGATA crystal, homogeneous distribution, or whether some register more than others, heterogeneous distribution. Because of the configuration of the detector-source system, some faces of the crystal are directly illuminated by the source, while others are located at the backside, i.e. some segments are located much closer to the source than others. The photons have easy access to some segments, while they have to pass through a greater thickness of the detector material to reach others. For this reason, the aim is to find out whether the photons reach all the segments in the same way, which would lead to a homogeneous distribution in the interactions with the crystal, or whether, on the contrary, there are some segments that are privileged over others. If the distribution is not homogeneous, during the experimental scanning, it would be necessary to perform different

43

sets of measurements by rotating the crystal, to characterise all the segments equally with sufficient statistics. In order to characterise the detector correctly, all the segments that make up the detector should be measured with enough statistics. Knowing the distribution of the detections, it is determined whether or not it is necessary to rotate the crystal during the experimental measurements, in order to increase the statistics.

· The average number of Compton and photoelectric processes in each event. Photons, when detected, do not deposit all their energy on the crystal in a single interaction, but undergo several Compton events in the same or different segments before being completely absorbed by the photoelectric effect. Through simulation it is possible to find the number of interaction processes for each event.

It should be noted that all these quantities are studied for the annihilation photons, which are the ones we are interested in, so an energy gate around 511 keV is set in both detectors.

4   Results and discussion

4.1   General horizontal 2D scanning

First, as already mentioned, a general scan is carried out in the horizontal plane with an ^{241}Am source. The objective of this scan is a primary characterisation of the slice 1, the lowest one, in order to propose a first location of the segment edges. In this way, the approximate position of the edges between segments is known, which allows a second, more rigorous scan to be done in the areas of interest. In other words, to be able to carry out a second, finer scan that provides more accurate results on the position of the edges, a previous, general scan is necessary to know where to search. Through the TkT programme, the spectra are plotted and the ^{241}Am peak is fitted to a Gaussian curve. For each position, the quotient between the peak area and the measurement time is calculated, and the values are plotted. The software used for the representation of the results is the programme Origin, which allows to plot and analyse a large set of data.

The results obtained from the general scanning with ^{241}Am are presented below, in a 3D plot in which the position coordinates are represented in the x and y axes and the count rate at each position in the z axis:
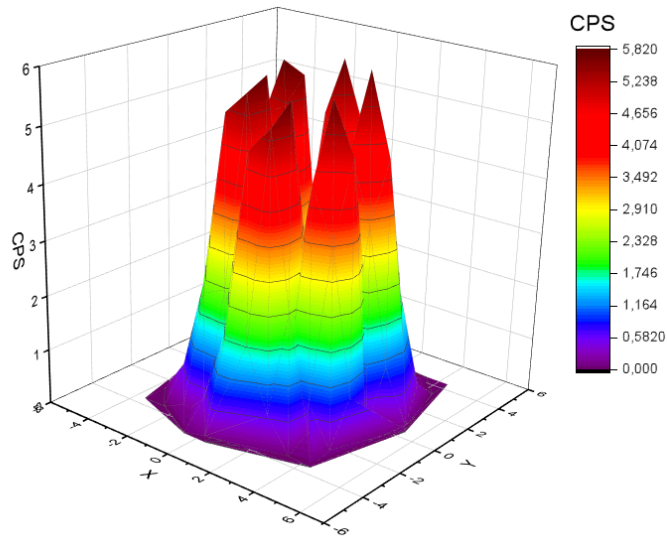
Figure 28: 3D representation of the number of counts obtained in each segment of the first ring as a function of position, in the first scan with ^{241}Am.

45
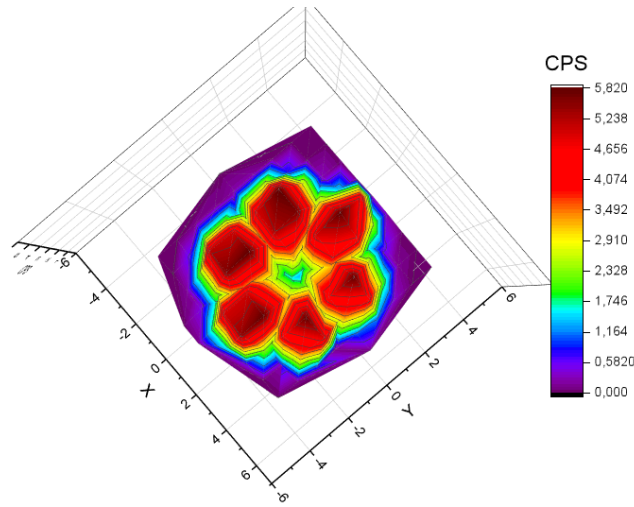
Figure 29: Horizontal projection of the figure 28.

The figure 28 shows the number of counts recorded by the segments of the first ring on the z-axis versus the position on the x- and y-axis (coordinates). In this way, graphically, a first idea of the real structure of the crystal is given, such as its active volume or the location of the edges between segments, all referring only to the first ring, the lower one. The figure 29 is more interesting as it allows us to propose a first location of the hole and the real position of the segments. Therefore, the next, more exhaustive, fine scan is performed on the regions of interest that can be found in this graph. In other words, the initial scan is used to propose a first structure of the crystal and to know the points to measure in the next scan.

As expected, the counting is the highest in the centre of the segments and decreases towards the outer edges of the crystal and at the boundaries between segments. This is how the edges between segments are located, because these are the areas where the counting decreases very significantly. As can be seen in figure 29, there are six portions, corresponding to the six segments, which present a similar structure, the counting is maximum in the centre and decreases towards the boundaries. Between these portions, there are straight areas where the number of counts per second is notably lower than in the rest of the space, so they are identified with the edges between segments. Once these boundaries are roughly located, a finer scan can be performed to provide more accurate results. In addition, the hole is very noticeable. It is an area where the γ rays are not detected, because there is no crystal, so the counting must be practically null at the corresponding points, and this is the behaviour that is clearly observed in the figure.

46

4.2   Specific horizontal 2D scanning for the determination of transverse segment edges

After the general scan, which gives a first idea of the distribution of the segments in the first layer, a more exhaustive scan is carried out to determine their position more precisely. The locations are selected based on the results of the previous scan.

For this purpose, four sets of measurements are made for each segment edge, as described in the section 3.5.2. That is, for each boundary, measurements are taken along four imaginary lines. To facilitate the analysis, the position on the x-axis or on the y-axis is fixed in each case. To illustrate the data obtained, the graphs corresponding to the results for the edge between segments a1 and b1 are shown as an example:
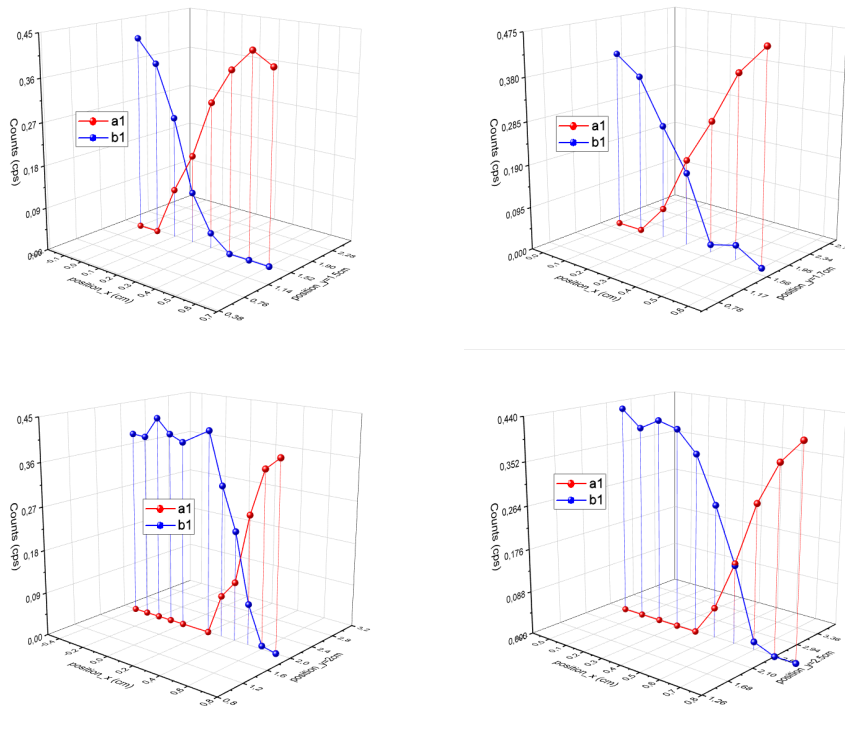
Figure 30: Representation of the results obtained during the exhaustive scanning of the boundary between segments a1 and b1, along four sets of measurements in which the position on the x-axis varies while keeping the value on the y-axis fixed. The data correspond to the measurement axes: $y = 1.5cm$ (top left), $y = 1.7cm$ (top right), $y = 2cm$ (bottom left), $y = 2.5cm$ (bottom right).

4.2 Specific horizontal 2D scanning for the determination of transverse segment edges

To determine the position of the edge between segments a1 and b1, measurements are taken along four lines, fixing, in this case, the y-axis on each of them: $y = 1.5cm$, $y = 1.7cm$, $y = 2cm$ and $y = 2.5cm$. From the graphs above, we can observe how the count in the segment a1 is maximum towards one end of the x-axis and decreases significantly towards the other one. The opposite behaviour is observed for segment b1. This shows the separation between segments: when the source is placed in such a position that the collimated beam is incident on segment a1, the count is maximum in this segment and minimum in b1. However, as we move along the x-axis towards segment b1, the number of counts recorded decreases in a1 and increases in b1, as expected. Therefore, by visualising the results through graphs, the theoretically proposed behaviour is verified. The point where the number of counts registered in segment a1 and b1 is the same, i.e. where the counting between a1 and b1 is equal, belongs to the boundary between these segments. For that reason, a linear fit is made for each segment with the closest points to that equilibrium position. The intersection of the two resulting line equations defines a point contained in the segment edge. A typical example of linear fit of the results, for segments a1 and b1, is shown below:
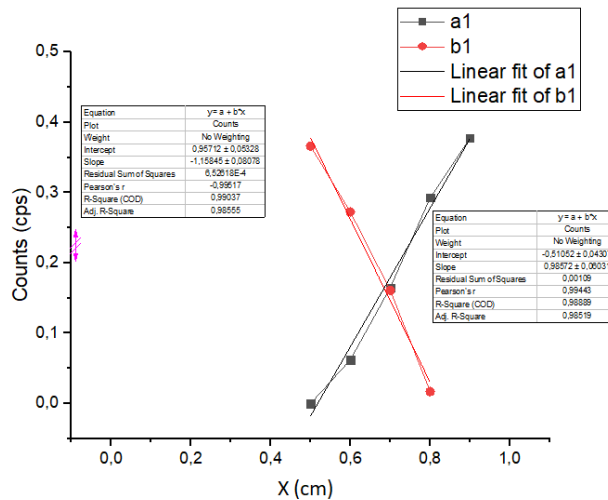
Figure 31: Linear fit of the experimentally obtained data on segments a1 and b1 when locating their separating edge, along the line y=2.5 cm.

The intersection of the two lines results in a point, actually we get the position on the x-axis because on the y-axis is fixed, where the counting is equal on both segments. It is therefore assumed that this point belongs to the edge between segments. The same procedure is performed with all data sets until the four points sought for each boundary are obtained.

For each segment edge there are four points belonging to that edge, derived experimentally through the data processing described recently. By means of the linear fit of these points, the equation that satisfies the boundary between segments is determined. The fit for the edge between a1 and b1 is then included:
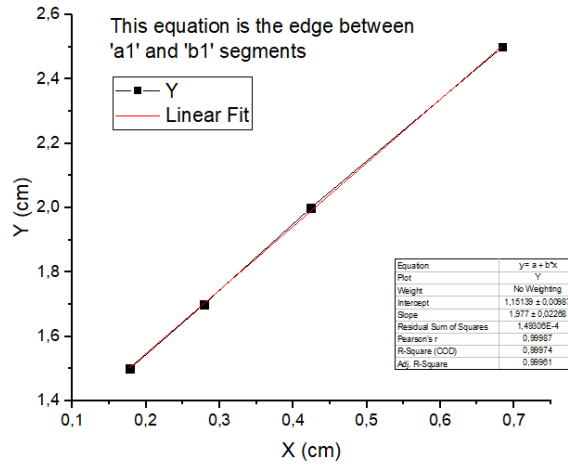
Figure 32: Linear fit of the points belonging to the edge between segments a1 and b1 to determine the equation satisfying this boundary.

In the same way, the results for the equations satisfying the rest of the boundaries, i.e. the edges b1-c1, c1-d1, etc., are obtained and included below (the linear fits for each boundary are incorporated in the annex A):

The equations being of the linear form: $y = a \cdot x + b$

Segment edge	Slope (a)	Intercept (b)	R-Square (COD)
a1-b1	1.98 ± 0.02	1.151 ± 0.010	0.9997
b1-c1	-1.44 ± 0.05	-0.59 ± 0.08	0.9973
c1-d1	0.0227 ± 0.0002	0.1790 ± 0.0004	0.9999
d1-e1	1.906 ± 0.011	1.15 ± 0.02	0.9999
e1-f1	-1.457 ± 0.012	-0.548 ± 0.005	0.9999
f1-a1	0.0498 ± 0.0006	0.2192 ± 0.0011	0.9997

Table 4: Data of the equations satisfying the segment boundaries in the first layer.

Finally, the distribution of the segments in the first layer is as follows:
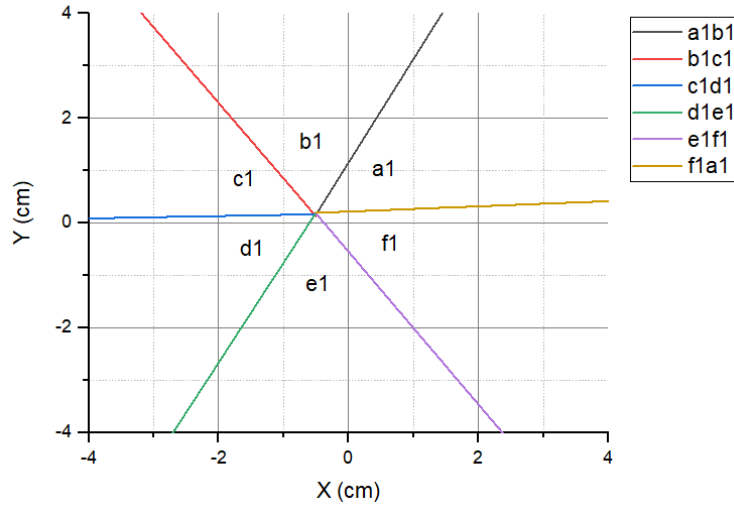
Figure 33: Distribution of the segments in the first layer through the representation of the boundaries between them.

4.3   Specific horizontal 2D scanning for the location of the central hole and its inclination

After determining the edges of the segments in the first layer, another scan is carried out to locate the position of the central hole and its alignment with respect to the vertical axis. To this aim, the analysis procedure described above 3.5.3 is performed.

Only the results obtained through the y-axis are included, since the scanning performed on the x-axis did not provide good results during analysis. Measurements on the x-axis shall be repeated after completion of the priority 3D scan.

As previously stated 3.5.3, the analysis consists of two data sets, one that groups the counting in three segments and one that groups the counting in the other three segments. The results are then combined according to position, in some cases the beam is closer to three of the segments forming a set and in other cases to the other three. Therefore, for each layer, the hole

is located by combining the results in the different segments. The values
obtained in each layer are shown below:
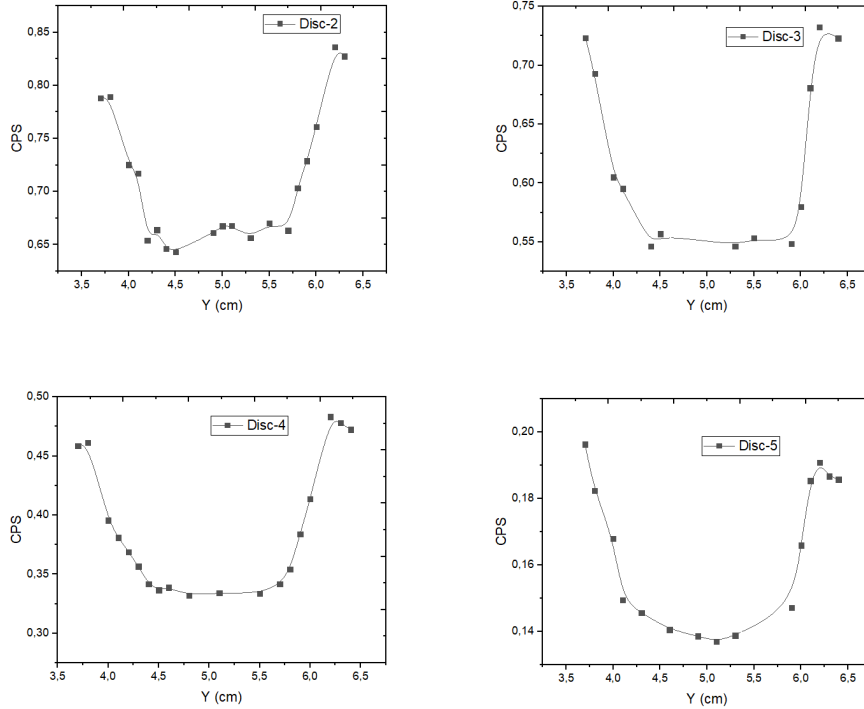
Figure 34: Representation of the number of counts versus the position on the y-axis to find
the location of the hole (its coordinate on the y-axis) in the different layers that constitute
the total detector. Layers: 2 (top left), 3 (top right), 4 (bottom left) and 5 (bottom right).

The following must be taken into account:

· In the first layer there is no central hole, as it starts from the second
  layer. Moreover, measurements do not give good results for the last
  layer, because most of the γ-rays are absorbed in the layers from 1 to
  5, so the statistics are very poor in the sixth one.

· The LRI-D is a low-radiation laboratory, so the sources that we use
  have low activity. For this reason, the results obtained are statistically
  poor, since increasing this parameter with low activity means extend-
  ing the measurement time significantly. To minimise the effect of the
  poor statistics, it is important to carry out a correct data treatment:
  results that deviate greatly from the general behaviour and that do not
  conform to the theoretical approach are discarded.

Then, for each layer, two linear fits are made with the results obtained
on both sides of the hole. That is to say, on the one hand, those points on
one side of the hole (fall) that follow an approximately linear behaviour are
fitted, and, on the other hand, those on the other side (rise). In this way,
two linear equations are obtained, the intersection of which gives the y-axis
coordinate of the central point of the hole. This gives the central points
(y-coordinate) of the hole in each layer. The experimental linear fits and the
intersections are given below:

Slice	Slope (a)	Intercept (b)	R-Square (COD)
2	-0.24 ± 0.03	1.70 ± 0.14	0.9282
	0.339 ± 0.012	-1.27 ± 0.07	0.9962
3	-0.34 ± 0.04	2.0 ± 0.2	0.9728
	0.65 ± 0.09	-3.3 ± 0.5	0.9633
4	-0.19 ± 0.02	1.16 ± 0.10	0.9371
	0.324 ± 0.010	-1.52 ± 0.06	0.9980
5	-0.108 ± 0.014	0.60 ± 0.05	0.9686
	0.15 ± 0.02	-0.74 ± 0.14	0.9544

Table 5: Linear fit data on both sides of the hole for each slice.

Slice	y-coordinate intersection (cm)
2	5.1 ± 0.4
3	5.4 ± 0.8
4	5.2 ± 0.3
5	5.2 ± 0.8

Table 6: Position of the hole in the y-axis in each slice.

By knowing the position of the hole in each layer, it is possible to deter-
mine whether the detector is tilted or not with respect to the vertical axis.
However, from the obtained results, no conclusion can be drawn about the
inclination of the central hole. The results derived from this scan are not
much accurate because of poor statistics. That is, since there are not enough
statistics in the measurement process, it is not possible to draw a conclusion
about the inclination of the hole, it cannot be assumed either that the de-
tector is tilted or not because the accuracy is very low. Therefore, in order
to carry out this study it is necessary to perform a more precise scan with
high statistics.

4.4   3D scanning - Experimental results

As far as the experimental part of the 3D scanning is concerned, we are in the data acquisition process, starting to measure. We have already prepared the coincidence setup, configuring the entire electronic installation so that it works correctly and make it possible to obtain the desired data. Among other controls, the energy thresholds have been set to optimise the signal-to-noise ratio. On the other hand, a series of problems related to the transmission of information from the different channels of the LYSO crystal of the γ-camera to the analysis software have been solved. The Go4 software, developed by GSI, is used for data collection. In this regard, we have learnt how to use this programme and configured the files to obtain the information we are interested in. Once all the experimental contingencies have been overcome, both at the electronic and software stages, we start measuring. The next future work consists of analysing these measurements in order to achieve useful results in the characterisation of the AGATA A005 capsule.

4.5   3D scanning - Geant4 simulation

The experimental 3D scanning setup is reproduced in a Geant4 simulation in order to determine certain magnitudes of interest that can be applied in the real experiment and to compare the results obtained in it. Among the properties of the system that are studied, the coincidence and individual efficiency of the detectors within the laboratory configuration, the distribution of detections between segments or the number of interaction processes in the detectors stand out. Section 3.7 introduces the two main parts that make up the simulation, the generation of data and the analysis of them to achieve useful results. In addition, figure 26 shows the detectors - source simulated configuration.

4.5.1   Individual and coincidence efficiency

Before including and discussing the results derived from the simulation, we estimate the geometric efficiency of the detectors in the proposed configuration. In other words, we calculate, approximately, the maximum efficiency that the detectors can achieve individually for geometric reasons. For this

purpose, the geometric efficiency is obtained as follows:

$$\varepsilon = \frac{\Omega}{4\pi} \tag{4}$$

Where Ω refers to the solid angle subtended by each detector, and 4π is the solid angle corresponding to the whole sphere.

To estimate the solid angle subtended by each detector, the equation below is employed:

$$\Omega = \frac{S}{R^2} \tag{5}$$

Where S designates the detector surface illuminated by the source and R the distance between the source and the detector.

Since the aim is to estimate the geometrical efficiency of the detectors in the experimental setup and not its rigorous determination, the detector surfaces are approximated as:

· The AGATA crystal surface is considered to be rectangular:

$$S_{AGATA} \sim 90 \cdot 65 \approx 5850 \; mm^2$$

· The detection surface of the γ-camera has a quadrangular shape thus it is determined as follows:

$$S_{\gamma-camera} = 104 \cdot 104 = 10816 \; mm^2$$

As for the distance between the source and the detectors, according to the experimental setup:
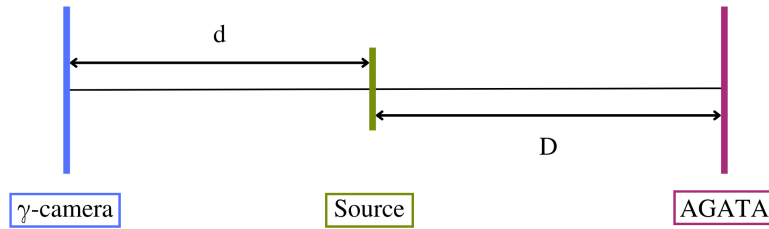
Figure 35: Schematic of the experimental setup recreated during simulation.

· Distance AGATA crystal - source: $D \sim 203.4 \; mm$

· Distance γ-camera - source: $d \sim 175.5 \; mm$

As it is an estimation, the thickness of the encapsulation is not taken into account for both detectors in the distance approach.

Therefore, the calculation of the respective solid angles leads to the following individual geometric efficiencies:

· AGATA crystal:
$$\Omega \sim \frac{5850 \ mm^2}{41372 \ mm^2} \approx 0.141 \ sr$$

$$\boldsymbol{\varepsilon \sim \frac{0.141}{4\pi} \approx 1.1\%}$$

· γ-camera:
$$\Omega \sim \frac{10816 \ mm^2}{30800 \ mm^2} \approx 0.351 \ sr$$

$$\boldsymbol{\varepsilon \sim \frac{0.351}{4\pi} \approx 2.8\%}$$

The geometrical efficiencies mark the limit in efficiency of each detector within the experimental setup. That is, if other factors such as the intrinsic efficiency of the crystals or the photon leakage of the detectors were not affected, the maximum efficiency values that could be reached would be the ones provided by the geometrical calculation. Consequently, although it is an estimation, the experimental efficiencies and those obtained by simulation cannot exceed 1.1% in the case of the AGATA crystal and 2.8% in the one of the γ-camera. These are very low values, and are the highest possible given the configuration of the system, so it is expected that the real efficiencies of the experiment and those from the simulation are extremely low. Therefore, it can be concluded that the proposed setup has a low efficiency because it is very limited by the small solid angle subtended by the detectors, among other reasons.

In the simulation, a certain number of events, i.e. ^{22}Na isotopes, are generated. For each event, a β^+ decay occurs, leading to the production of a ^{22}Ne particle in an excited state, a positron (e^+) and an electron neutrino (ν_e). The ^{22}Ne ions that are produced are in an excited state and decay to the fundamental one, emitting a photon of 1274.577 keV. Meanwhile, the positrons annihilate with the electrons from the medium and create two collinear 511 keV photons emitted in opposite directions. Therefore, for each ^{22}Na ion, i.e.

for each event, two 511 keV photons are generated. It is important to note that the analysis code is designed in such a way that only detected photons depositing an energy around 511 keV are considered. In effect, an energy gate is assumed for each detector in the range 505-517 keV, so that only 511 keV photons that are completely absorbed in the detectors are counted. Consequently, only the contribution of the 511 keV photons that deposit all their energy in the detectors is counted in the calculation of the efficiency or the distribution between segments; those that escape after experiencing some Compton scattering are not taken into account for the counting.

The results obtained for efficiency through simulation are included below:

Detectors working individually

The input data and the obtained results are presented, as well as the efficiency calculation:

N. of generated events	10000000
N. of 511 keV generated photons	20000000
N. of 511 keV photons detected in AGATA crystal	94936
N. of 511 keV photons detected in γ-camera	58412

Table 7: Simulation input and output values.

The efficiency is calculated using the relation:

$$\varepsilon_{511} = \frac{N. \ of \ 511 \ keV \ photons \ detected}{N. \ of \ 511 \ keV \ photons \ generated} \tag{6}$$

Therefore, the individual efficiencies result:

· AGATA crystal:
$$\boldsymbol{\varepsilon_{511} = 0.47 \ \%}$$

· γ-camera:
$$\boldsymbol{\varepsilon_{511} = 0.29 \ \%}$$

Based on the values obtained, it can be noticed that the efficiencies of the individual detectors are extremely low, since none of them exceeds 0.50%. However, this is to be expected because the efficiency in this system is very

56

limited by the reduced solid angle and conditioned by the complete absorption of the photons. Furthermore, it is verified that the efficiencies determined by simulation are lower than those estimated by geometry, as expected. The geometrical efficiencies were already very small, so it was expected that the efficiencies calculated through equation 6, with the simulation results, would be extremely low. Moreover, it is noted that the efficiency of AGATA is higher than that of the LYSO crystal in the γ-camera, and this may be due to the fact that the active detection volume of the first one is higher than that of the second one.

Detectors operating in coincidence

The experimental study is carried out with the detectors operating in coincidence, so what really matters is to calculate the efficiency of the system in coincidence. In the simulation, it is assumed that two photons are detected in coincidence if they are part of the same event. In other words, when the two annihilation photons generated in one event are detected in both detectors, an event in coincidence is added. The results are shown in the following table:

N. of generated events	10000000
N. of coincidences	12471

Table 8: Simulation input and output values.

The efficiency is found through the equation:

$$\varepsilon_{coincidence} = \frac{N.\ of\ coincidences}{N.\ of\ events}$$

Indeed, the coincidence efficiency is calculated as the number of events detected in coincidence in comparison with the total, or, in other words, the number of photons detected in coincidence divided by the total number of them produced. The ratio is the same since the difference between one method and the other is a factor of 2 in both the numerator and the denominator, keeping the fraction invariant. Therefore,

$$\varepsilon_{coincidence} = \mathbf{0.12\ \%}$$

As expected, the efficiency of the detectors working in coincidence is very low, just about 0.12%. This is an extremely small value, indicating that only a reduced number of photons are detected in coincidence out of all the photons generated, 12 out of 10000. Nevertheless, it is to be expected that the efficiency in coincidence is so low since the efficiencies of the detectors operating individually are very small, and this is supplemented by the coincidence condition. The coincidence condition limits the value of the efficiency, decreasing it with respect to the individual case. It should be noted that, under this condition, only the 511 keV photons that reach the detectors simultaneously, i.e. in the same event, and are completely absorbed by both, are taken into account.

The small solid angle subtended by the detectors is the main cause of the low efficiency of the experimental system. However, there are other phenomena that limit the efficiency of the setup, such as the intrinsic efficiency of the detectors, although this is not taken into account in the simulation. On the other hand, the analysis code establishes an energy gate around 511 keV, so only those events in which the photons are completely absorbed in the detectors are considered, i.e., if after experiencing some Compton process they escape from the detector, these events are rejected and are not added to the count. Thus, the efficiency is also limited by the total absorption of photons in the detectors. If, in addition to all these limitations on the individual detectors, the coincidence condition is included, the efficiency of the system is expected to decrease to a very small value.

This leads to the conclusion that, as expected given the experimental setup, the efficiency of the system in coincidence is very low. In addition, the individual detector efficiencies are also very poor due to the distribution of the experiment.

4.5.2   Distribution between segments

As mentioned above, the aim of the simulation is to obtain results applicable to the real experiment. That is, to use the knowledge provided by the simulation to the laboratory experience. For this reason, the purpose is to determine how the photon detection is distributed among the different segments. The experimental configuration consists of placing the ion source between the two detectors with all the elements aligned, so that some segments are located closer to the source than others. Therefore, we raise the

possibility that photons interact more easily in the segments closest to the source while they have more difficulty reaching those on the other side, since they would have to pass through the entire volume of the crystal to reach them, passing through other segments. Nevertheless, this effect could be practically irrelevant and photons could be distributed uniformly throughout the detector. In the first case, it would be necessary to take several sets of measurements by rotating the crystal around its vertical axis, so that all segments are characterised equally, with the same statistics. However, if the distribution was homogeneous, it would not be required to rotate the capsule because all segments would be triggered equally. For this reason, it is important to know how the photon detections are distributed among the different segments that make up the crystal.

In the analysis code, an energy gate between 505 and 517 keV is set to select the annihilation photons that are completely absorbed in the crystal. Although the total energy deposited in the detector has to be around 511 keV, photons can interact in different segments, losing a part of their energy in each of them. That is, in general, photons do not deposit all their energy in the same segment but involve two, three or more segments for their detection. For this reason, we calculate the proportion of energy deposited by each photon in each segment. For example, if a photon deposits 70% of its energy in one segment and 30% in another, 0.7 is added to the count of the first segment and 0.3 to the counting of the second, so that for each photon one unit is added to the total count of the crystal and the proportional part to the count of the individual segments, always normalised to 1 per photon. It should be remembered that we are studying the distribution of detections, not interactions. That is, for each photon there can be one detection in the crystal, but multiple interactions. At the end, the sum of all the segments must correspond to the total number of detections in the whole crystal.

We generate 10000000 events, through which the following results are achieved for the distribution between segments:

Slice / Seg.	1	2	3	4	5	6
1	647.37	1289.55	2080.19	1987.17	1214.33	672.04
2	718.62	1662.05	2857.58	2607.87	1589.50	780.09
3	1229.59	2658.60	4563.91	4255.45	2560.85	1277.03
4	1529.65	3455.06	6054.88	5624.57	3149.01	1531.53
5	1409.93	3509.02	6695.48	5902.55	3183.77	1481.44
6	1014.45	2653.18	5185.87	4556.90	2326.27	1020.23

Table 9: Distribution of the 511 keV photons detected in the AGATA crystal among the different segments. The first column shows the slices while the first row indicates the segments.

As can be inferred from the table above, the distribution is not homogeneous between segments. We observe that some segments, such as 5-3, 4-3, or 5-4, have a large number of photon detections while others, such as 1-1, 1-6, or 2-1, are hardly reached by them. This shows that the segments closest to the source absorb most of the photons detected by the crystal while the farthest ones, those on the opposite side of the source, are hardly fired at all. This result is expected because, in order to reach the farthest segments, photons have to pass through the material of the front segments, i.e. a greater thickness, than the nearest ones. Consequently, to analyse all segments with similar statistics and for the AGATA crystal to be correctly characterised, it is necessary to take several sets of measurements at each position. In other words, the capsule has to be measured by rotating around its axis to expose different sides of the crystal to the source, and thus different segments, in order to increase the statistics.

4.5.3   Average number of interactions in detectors

Finally, we study the average number of interactions of each photon per detection, i.e. the number of Compton plus photoelectric processes that photons undergo before being completely absorbed in the detectors. As for the other quantities, only the 511 keV photons that are completely absorbed are taken into account. To calculate the average number of interactions per detection, we determine the total number of interactions in each detector and we divide it by the number of detected photons. This quantity gives an idea of the number of steps, events, that the photons experience in the detectors until they are completely absorbed and is, therefore, an indicator of the degree of difficulty of the position reconstruction by trajectory.

Then, for each detector, we seek to obtain the ratio $N_{interactions}/N_{detections}$. The obtained data are presented in the table below:

N. of generated events	10000000
N. of 511 keV photons detected in AGATA crystal	94936
N. of 511 keV photons detected in γ-camera	58412
N. of interactions corresponding to these detections in AGATA crystal	1009735
N. of interactions corresponding to these detections in γ-camera	578866

Table 10: Simulation input and output values.

By employing the relation described above, the following results are derived:

· AGATA crystal:
$$\mathbf{N_{int}/N_{det} = 10.64}$$

· γ-camera:
$$\mathbf{N_{int}/N_{det} = 9.91}$$

From the results it follows that approximately 10 interactions occur per detection, both in the AGATA crystal and in the γ-camera. That is, on average, for each detection, 9 Compton scattering processes take place plus one total absorption to end. As can be observed, although in both detectors the average is around 10, in the AGATA crystal there are, in general, more interactions per detection than in the LYSO of the γ-camera. The higher this ratio, the more complicated it is to reconstruct the emission position per trajectory, since it involves a larger number of stages. It is therefore desirable that this relation is as small as possible, in order to make the reconstruction the easiest possible.

4.5.4   Histograms

The energy deposited by the photons in each detector is collected in histograms, so that a spectrum is obtained from the AGATA crystal and another from the γ-camera. In addition, a histogram representing the coincidences between the two detectors is also generated. These spectra are included below:

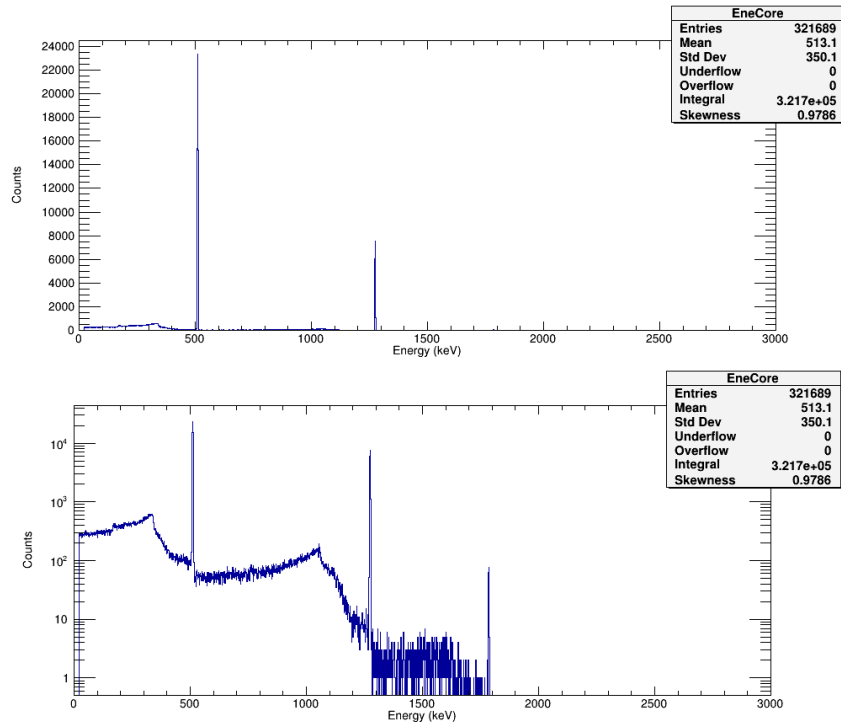Figure 36: Spectrum provided by the AGATA crystal (top in linear scale, bottom in logarithmic scale).
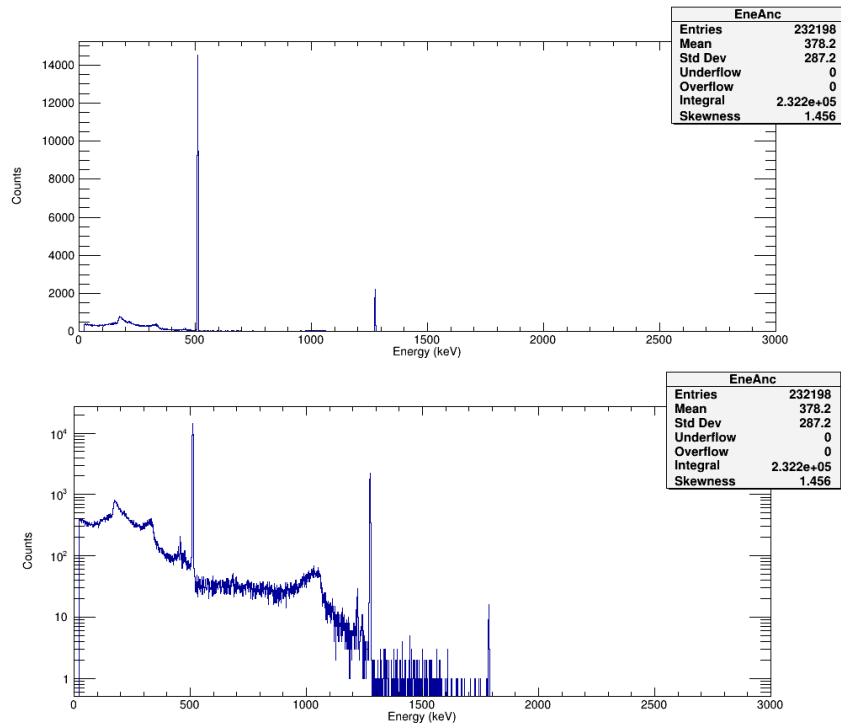
Figure 37: Spectrum measured with the γ-camera (top in linear scale, bottom in logarithmic scale).
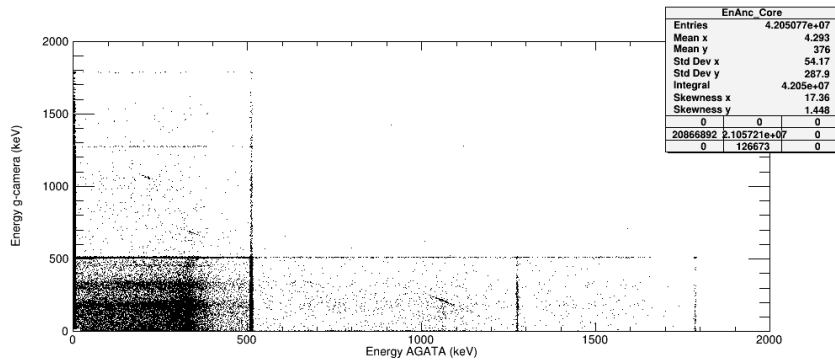

Figure 38: Representation of the coincidences between the AGATA crystal and the γ-camera. It is a 2D histogram in which the energies of the photons recorded by the detectors are plotted on both axes.

63

First of all, it is important to mention that in order to obtain the AGATA spectra, the LYSO crystal one and the coincidence representation, all the information about the detected particles is incorporated in the histograms, i.e. no energy gate is fixed, but everything recorded by the detectors is plotted.

In the AGATA and γ-camera spectra, the total absorption peaks produced by the presence of the ^{22}Na source are the most remarkable. Indeed, the one at 511 keV is caused by the energy of the annihilation photons, the one at 1275 keV is due to the desexcitation of ^{22}Ne and the one at 1786 keV corresponds to the sum peak of the previous emissions. Furthermore, on a logarithmic scale it is possible to discern the continuum and the Compton edge generated by the 511 and 1275 keV photons.

In addition to the peaks and background due to the ^{22}Na source, in the spectrum generated by the γ-camera, we also observe peaks caused by the intrinsic activity of LYSO. As discussed in section 1.4, the LYSO crystal contains an unstable isotope, ^{176}Lu, which emits radiation that is detected in the crystal itself. For this reason, peaks appear at the energies corresponding to these emissions, 202 and 307 keV. This is one of the main differences between the AGATA spectrum and the γ-camera one.

Finally, the histogram recording the coincidences between the two detectors is analysed. The x-axis represents the energy in the AGATA capsule while the y-axis includes the information about the γ-camera. In figure 38, all hits that are measured in coincidence, i.e. in the same event, are plotted. It can be observed that a large number of them occur when a photon of either 511 or 1274 keV is completely absorbed in the detector which triggers. Likewise, a high number of coincidences are generated by Compton processes, photons that are not fully absorbed but deposit part of their energy in the detectors, as observed in the region between 0-511 keV on both axes. However, among all the events in which photons are detected simultaneously, we are only interested in those in which the 511 keV γ´s are completely absorbed. That is, from the whole set of possibilities in coincidence, we restrict the study to those events in which the annihilation photons are fully absorbed.

4.6 Resolution analysis

The resolution of the detectors is one of the key magnitudes in the AGATA spectrometer. For this reason, we carry out a study analysing this quantity of the A005 capsule in our system when digital and analogue electronics are used. The obtained results are compared with those achieved by other research groups in the collaboration many years ago. For this purpose, we employ different radioactive sources, which logically provide diverse peaks in the spectra depending on their emissions. See annex B for the calculation of the resolution.

We carry out the measurements using the electronics as follows:

· Analogue: The MDR to BNC converter is used for getting the signal from the detector to the amplifier. To perform the measurement, we employ the ORTEC 575A spectroscopic amplifier, which provides the shaping time of interest for the process, the 3 μs one. For the data acquisition, the EASY-MCA-8K is used, whereas the software MAESTRO is employed for the analysis of the spectra. Through this software, it is easy to obtain the FWHM values of the concerning peaks.

· Digital: Regarding the electronics, the AGATA ones described above are employed while the TkT software is used for the analysis of the spectra. To determine the FWHM of each peak, we take advantage of the Gaussian fitting tool that directly provide this quantity.

As for the sources, we examine the 1332.492 keV emission from ^{60}Co and the 59.54 keV one from ^{241}Am.

The results obtained in our laboratory are compared with those achieved at the University of Liverpool and those provided by the Canberra group, and are included below:

4.6.1 From the 1332.492 keV emission of ^{60}Co

The results are plotted:

Figure 39: Resolution of the A005 capsule from the 1332.492 keV emission of ^{60}Co. The FWHM value of the 1332.492 keV peak is plotted against the segments where it is detected. The results belong to the Canberra group (purple), the University of Liverpool (green) and the University of Salamanca, digital electronics (orange) and analogue (yellow).

The graph shows the values obtained in the segments, for consulting numerical figures see appendix C. As concerns the core, the results are shown below:

Core	FWHM (keV)
Canberra	2.17
University of Liverpool	2.24
University of Salamanca (digital)	2.77
University of Salamanca (analogue)	2.77

Table 11: FWHM values in the core for the 1332.492 keV emission of ^{60}Co

First of all, it should be noted that the FWHM values are compared directly rather than calculating the resolution from them. That is because they are studied for a given emission at a given energy. In other words, as the comparisons are made individually for one emission, the photopeak energy

66

is the same in all cases, it does not vary, and, for this reason, it is indifferent to analyse the FWHM or the resolution.

As a general behaviour, it can be observed that the Canberra company (manufacturer of the detector) is the one that achieves the best resolutions in the different segments, since it is the one that obtains the lowest FWHM values. As for Liverpool and Salamanca, the method followed by the first ones gives better results for the resolution, although in some cases the values are very similar. However, the results from Canberra and Liverpool are old data, as they were obtained years ago. A comparison between the two types of electronics shows that the variations in resolution between segments are much greater, more significant in the case of analogue than in digital ones. It means, digital electronics provide much more stable results between segments while analogue electronics fluctuate more. Nevertheless, all the results from the different groups are collected in the same range, so it can be assumed that the resolution of the A005 capsule segments for the 1332.492 keV energy emission of ^{60}Co is between 1.8 - 2.6 keV, in terms of FWHM.

Regarding the core, the difference between the results in Salamanca with respect to Canberra and Liverpool is much larger than in the segments. Although the values of the last two groups are within the range mentioned above, the results achieved in Salamanca do not belong to this interval. For the core, the FWHM obtained in Salamanca is notably higher.

4.6.2 From the 59.54 keV emission of ^{241}Am
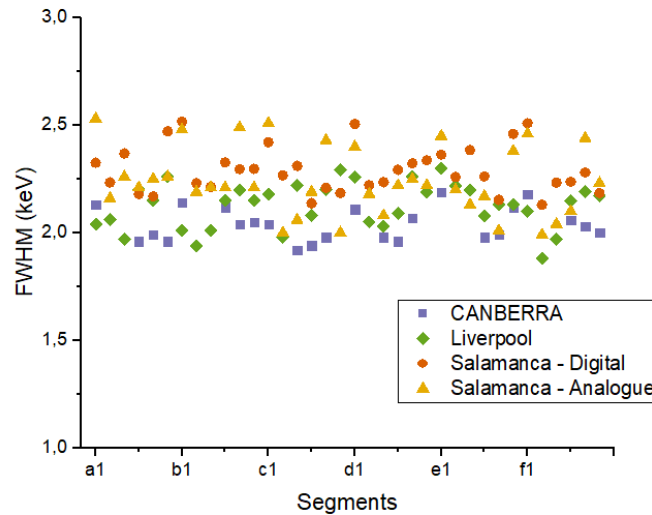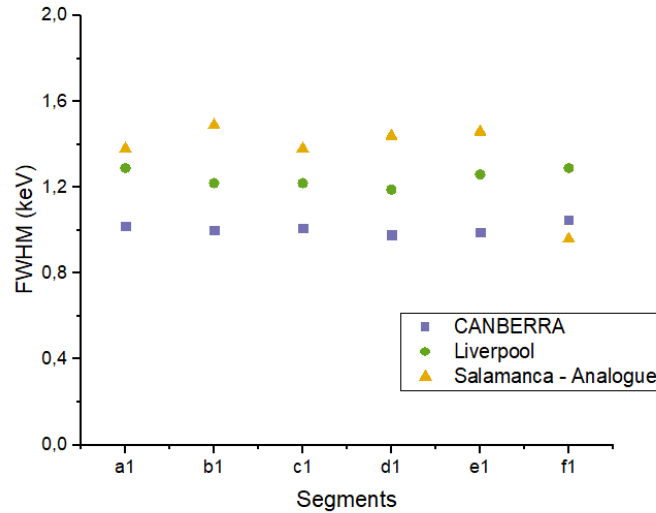
The values obtained are represented:

Figure 40: Resolution of the A005 capsule from the 59.54 keV emission of ^{241}Am. The FWHM value of the 59.54 keV peak is plotted against the segments where it is detected. The results belong to the Canberra group (purple), the University of Liverpool (green) and the analogue electronics of the University of Salamanca (yellow).

As for the core, we do not have data for the 59.54 keV emission of ^{241}Am from the Canberra company and from the University of Liverpool. In Salamanca, the FWHM value obtained in the core with analogue electronics is: $FWHM = 1.66\ keV$.

For this emission, we have only carried out the study with analogue electronics. At the end of the experiment, if necessary, the digital analysis will be performed. All numerical values are tabulated in annex C.

To begin with, it is important to remember that the γ emission of ^{241}Am is very low energy (59.54 keV), so the photons are absorbed at shallow depth, i.e. in the first slice of the capsule. For that reason, we only have data from the lower slice, the one closest to the source, because most of the photons are absorbed there and do not reach the upper segments. That is why we only have sufficient statistics on the segments of the first slice, and these are the ones we analyse with this emission.

As with the ^{60}Co emission, the best values for the resolution are obtained through the analysis of the Canberra group, followed by the University of Liverpool and the University of Salamanca. On the other hand, it is observed that, within the results of each group, there is hardly any variation between segments. That is, the resolution achieved in the different segments of the first slice is practically the same. Finally, the resolution, in terms of FWHM, of the segments of the first slice for the ^{241}Am emission is in the range of approximately 1 - 1.6 keV, better than the one for ^{60}Co.

5   Conclusions

The AGATA project consists of the design and development of an innovative spectrometer based on the tracking technique for γ-ray detection. In addition to this tool, it incorporates important advances in crystal segmentation technology, which makes it possible to cover a larger solid angle and achieve unprecedented values of efficiency and angular resolution. Because of its excellent characteristics, due to the technological advances it includes, it is intended to be used in nuclear structure research experiments, such as studies of exotic nuclei and their energy levels, nuclear force analysis, etc.

Before including the capsules in the spectrometer structure, it is necessary to characterise their response, so that they can operate and be used correctly. This work describes the characterisation of the A005 capsule through 2D and 3D scans. In addition to being a preliminary step to the nuclear structure experiments for which the spectrometer has been designed, the characterisation of the capsule also allows a comparison of the different methods and scanning tables of the groups involved in this stage of the collaboration.

The characterisation is mainly divided into two scans, first the 2D scan and then the 3D one. A 2D scanning method is designed to determine the real distribution of the detector inside the capsule, i.e. the position occupied by the segments and their active volume. For this purpose, we use a ^{241}Am source to locate the axes and a general and a specific scan is performed on the areas of interest. On the other hand, we employ ^{60}Co and ^{137}Cs sources to establish the position of the central hole and its inclination. In the light of the results, it is inferred that the low statistics of the measurements are sufficient to locate the segment boundaries, but no conclusion can be drawn about the detector tilt because of the lack of statistical accuracy. The proposed method would be appropriate if more intense sources (LRI-D is a low radiation laboratory) or more measurement time were available, so that the statistics would improve. In order to carry out a reliable study about the inclination of the central hole, it is necessary to perform a more accurate scan with high statistics.

In second place, a 3D scanning method is proposed to investigate the electrical response of the detector at different photon interaction positions. Taking advantage of the collinearity of the annihilation photons from a ^{22}Na source, an experimental setup is designed employing two detectors which operate in coincidence, the one to be scanned and a complementary γ-camera.

The distinctive feature of the scanning compared to what is carried out in other research groups is that we use active collimation and pulse shape analysis (PSA) techniques. That is, the aim is to know the response of the detector at each interaction point in order to be able to reconstruct the trajectory of the photons and the position from which they are emitted.

While the experimental coincidence setup is being fine-tuned, we carry out a simulation that recreates the real laboratory distribution. Through it, different magnitudes of interest are studied because its results provide an idea of what can be expected at the experimental stage. On the one hand, it is found that the efficiencies of the detectors operating individually are very low, lower than those estimated geometrically, as expected. Moreover, the efficiency in coincidence is also very poor, just about 0.12%. The main feature limiting the efficiency is the reduced solid angle subtended by the detectors, although other factors such as the total absorption of the photons also affect it. On the other hand, we study the distribution of detections among AGATA segments, and conclude that it is not homogeneous. The photons are mostly absorbed in the segments closest to the source, and only a few reach the farthest ones as they have to penetrate the entire detector. Therefore, during the experimental measurements it is necessary to rotate the capsule so that all segments are properly and equally characterised. Finally, we determine that, in both detectors, approximately 10 interactions of the annihilation photons occur per detection. It should be remembered that all these results are restricted to the condition of total absorption of the annihilation photons in the detectors, because we establish energy gates around 511 keV (505-517 keV) in them.

As mentioned before, one of the main challenges facing the AGATA spectrometer is to achieve significant progress in terms of spatial resolution, which is a fundamental magnitude in this detector. Through the corresponding study, we provide current data on the resolution of the A005 capsule, since those of the Canberra group and the University of Liverpool were reported years ago. However, their analysis seems to produce better results. Furthermore, there are no significant variations between the different segments within the same procedure, within a group. That is, the resolution achieved in all segments is practically the same. Numerically, taking into account the different segments, the FWHM value is in the range of 1.8-2.6 keV for ^{60}Co (1332.492 keV), and 1-1.6 for ^{241}Am (59.54 keV, only first slice).

A   Results of specific horizontal 2D scanning

The final linear fits made for the determination of the transverse segment boundary equations are given below:
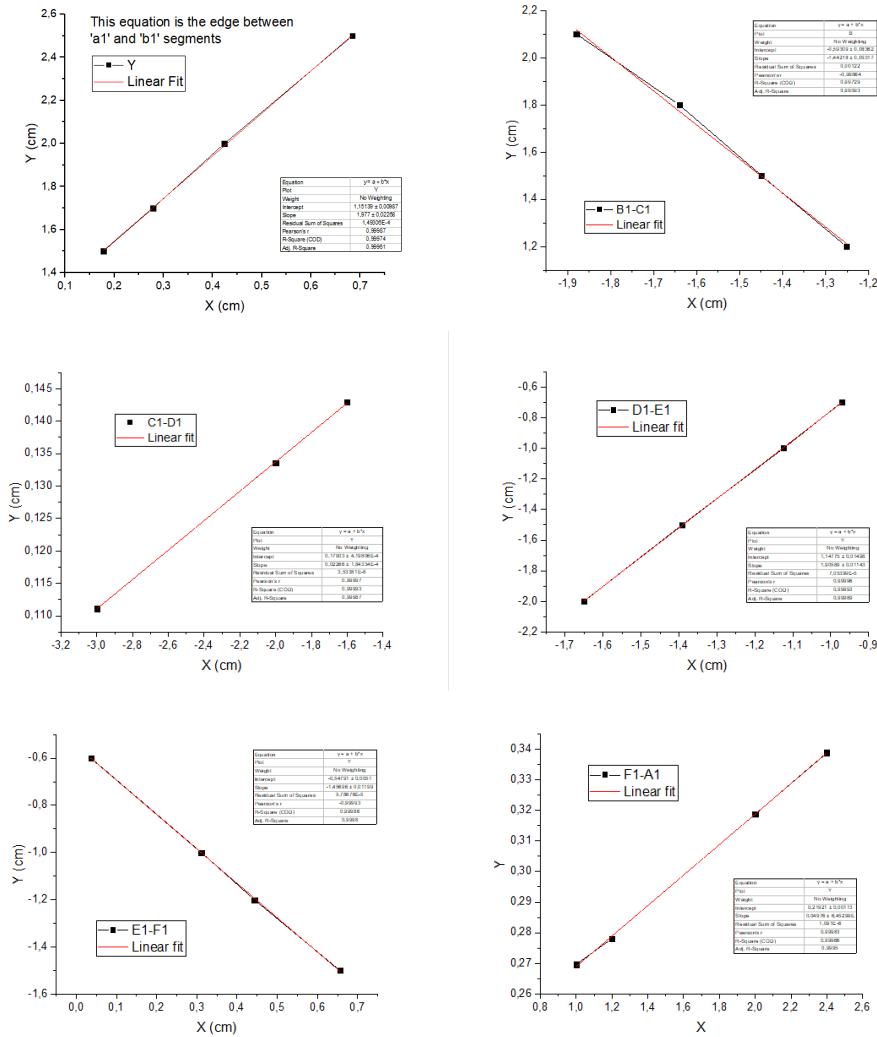

Figure 41: Linear fit of the points belonging to the edge between segments to determine the equation satisfying these boundaries. In each graph, the segments separating the edge are specified, i.e., a1-b1 top left, b1-c1 top right, etc.

B Calculation of resolution

The resolution in a Gaussian distribution is calculated as follows:

$$Resolution = \frac{FWHM}{E_0} \tag{7}$$

where E_0 is the centroid of the distribution, in this case the photon energy corresponding to the radioactive emission of the source, and FWHM (Full Width at Half Maximum) refers to the width of the respective peak measured at half maximum.
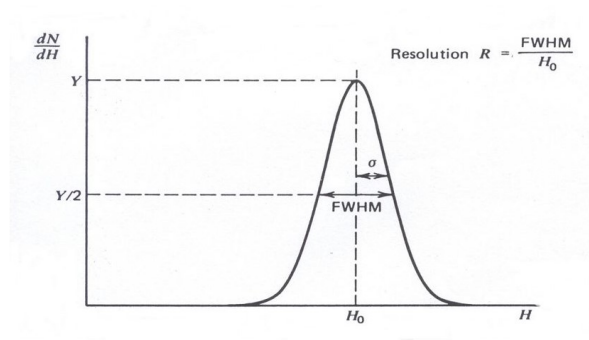

Figure 42: Gaussian curve showing the centroid (E_0) and the width at half-height (FWHM).

The FHWM is related to the standard deviation of the distribution so that:

$$FWHM = 2\sqrt{2ln2}\sigma \approx 2.355\sigma \tag{8}$$

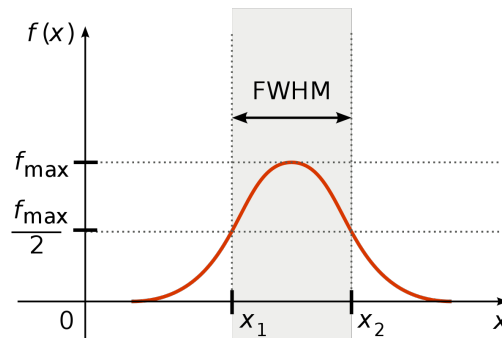where σ is the standard deviation.

Figure 43: Gaussian curve showing the meaning of the quantity FWHM.

C Resolution figures

We include below the resolution values, FWHM (keV), obtained by the Canberra group, the University of Liverpool and the University of Salamanca (with both digital and analogue electronics) through the 1332.492 keV emission of ^{60}Co.

Segment	Canberra	Liverpool	Digital Electronics	Analogue Electronics
Core	2.17	2.24	2.77	2.77
a1	2.13	2.04	2.33	2.53
a2		2.06	2.23	2.16
a3		1.97	2.37	2.26
a4	1.96	2.20	2.18	2.21
a5	1.99	2.15	2.17	2.25
a6	1.96	2.26	2.47	2.26
b1	2.14	2.01	2.52	2.48
b2		1.94	2.23	2.19
b3		2.01	2.21	2.21
b4	2.12	2.15	2.33	2.21
b5	2.04	2.20	2.30	2.49
b6	2.05	2.15	2.30	2.21
c1	2.04	2.18	2.42	2.51
c2		1.98	2.27	2.00
c3	1.92	2.22	2.31	2.06
c4	1.94	2.08	2.14	2.19
c5	1.98	2.20	2.21	2.43
c6		2.29	2.19	2.00
d1	2.11	2.26	2.51	2.40
d2		2.05	2.22	2.18
d3	1.98	2.03	2.24	2.08
d4	1.96	2.09	2.29	2.22
d5	2.07	2.26	2.32	2.25
d6		2.19	2.34	2.22
e1	2.19	2.30	2.36	2.45
e2		2.22	2.26	2.20
e3		2.20	2.38	2.13
e4	1.98	2.08	2.26	2.17

Segment	Canberra	Liverpool	Digital Electronics	Analogue Electronics
e5	1.99	2.13	2.15	2.01
e6	2.12	2.13	2.46	2.38
f1	2.18	2.10	2.51	2.46
f2		1.88	2.13	1.99
f3		1.97	2.23	2.04
f4	2.06	2.15	2.24	2.10
f5	2.03	2.19	2.28	2.44
f6	2.00	2.17	2.18	2.23

Table 12: FWHM (keV) values for the 1332.492 keV emission of ^{60}Co.

As for the 59.54 keV emission of ^{241}Am, the resolution values, FWHM (keV), are incorporated below:

Segment	Canberra	Liverpool	Analogue Electronics
Core			1.66
a1	1.02	1.29	1.38
b1	1.00	1.22	1.49
c1	1.01	1.22	1.38
d1	0.98	1.19	1.44
e1	0.99	1.26	1.46
f1	1.05	1.29	0.96

Table 13: FWHM (keV) values for the 59.54 keV emission of ^{241}Am.

Bibliography

[1] Ha, T., Korichi, A., le Blanc, F., Désesquelles, P., Dosme, N., Grave, X., Karkour, N., Leboutelier, S., Legay, E., Linget, D., Travers, B., & Pariset, P. (2013). *New setup for the characterisation of the AGATA detectors.* Nuclear Instruments and Methods in Physics Research Section A: Accelerators, Spectrometers, Detectors and Associated Equipment, 697, 123–132. https://doi.org/10.1016/j.nima.2012.08.111

[2] Nelson, L., Dimmock, M., Boston, A., Boston, H., Cresswell, J., Nolan, P., Lazarus, I., Simpson, J., Medina, P., Santos, C., & Parisel, C. (2007). *Characterisation of an AGATA symmetric prototype detector.* Nuclear Instruments and Methods in Physics Research Section A: Accelerators, Spectrometers, Detectors and Associated Equipment, 573(1–2), 153–156. https://doi.org/10.1016/j.nima.2006.11.042

[3] Ginsz, M. & Duchêne, G. (2015). Tesis doctoral *Caractérisation de détecteurs multi-segmentés au germanium hyper pur.* Université de Strasbourg. Ecole doctorale de physique et chimie physique. Institut pluridisciplinaire Hubert Curien.

[4] Akkoyun, S., Algora, A., Alikhani, B., Ameil, F., de Angelis, G., Arnold, L., Astier, A., Ataç, A., Aubert, Y., Aufranc, C., Austin, A., Aydin, S., Azaiez, F., Badoer, S., Balabanski, D., Barrientos, D., Baulieu, G., Baumann, R., Bazzacco, D., . . . Zucchiatti, A. (2012). *AGATA—Advanced GAmma Tracking Array.* Nuclear Instruments and Methods in Physics Research Section A: Accelerators, Spectrometers, Detectors and Associated Equipment, 668, 26–58. https://doi.org/10.1016/j.nima.2011.11.081

[5] Goel, N., Domingo-Pardo, C., Habermann, T., Ameil, F., Engert, T., Gerl, J., Kojouharov, I., Maruhn, J., Pietralla, N., & Schaffner, H. (2013). *Characterisation of a symmetric AGATA detector using the imaging scanning technique.* Nuclear Instruments and Methods in Physics Research Section A: Accelerators, Spectrometers, Detectors and Associated Equipment, 700, 10–21. https://doi.org/10.1016/j.nima.2012.10.028

[6] Hernández, A. & Quintana, B. (2016). Tesis doctoral *SALSA: Un sistema de caracterización de la respuesta eléctrica de detectores de germanio hiperpuro con contactos segmentados basado en una cámara γ de alta resolución.* Universidad de Salamanca. Instituto de Física Fundamental y Matemáticas. Laboratorio de Radiaciones Ionizantes

[7] Hernandez-Prieto, A., & Quintana, B. (2013). *Characterization of a High Spatial Resolution γ Camera for Scanning HPGe Segmented Detectors.* IEEE Transactions on Nuclear Science, 60(6), 4719-4726. https://doi.org/10.1109/tns.2013.2287252

[8] Debertin, K., & Helmer, R. G. (1988). *Gamma- and X-ray Spectrometry with Semiconductor Detectors.* North-Holland.

[9] Spieler, H. (2005). *Semiconductor Detector Systems.* Oxford University Press.

[10] Alva-Sánchez, H., Zepeda-Barrios, A., Díaz-Martínez, V. D., Murrieta-Rodríguez, T., Martínez-Dávalos, A., & Rodríguez-Villafuerte, M. (2018). *Understanding the intrinsic radioactivity energy spectrum from 176Lu in LYSO/LSO scintillation crystals.* Scientific Reports, 8(1). https://doi.org/10.1038/s41598-018-35684-x

[11] NUCLÉIDE-LARA on the web (2022). http://www.nucleide.org/Laraweb/index.php